DEPARTMENT OF MECHANICAL ENGINEERING & MECHANICS
COLLEGE OF ENGINEERING & TECHNOLOGY
OLD DOMINION UNIVERSITY
NORFOLK, VIRGINIA 23529

METHODOLOGY FOR SENSITIVITY ANALYSIS, APPROXIMATE ANALYSIS, AND DESIGN OPTIMIZATION IN CFD FOR MULTIDISCIPLINARY APPLICATIONS

By

Arthur C. Taylor III, Principal Investigator
Gene W. Hou, Co-Principal Investigator

Progress Report
For the period April 15, 1991 to April 14, 1992

April 1992

Old Dominion University Research Foundation

DEPARTMENT OF MECHANICAL ENGINEERING & MECHANICS
COLLEGE OF ENGINEERING & TECHNOLOGY
OLD DOMINION UNIVERSITY
NORFOLK, VIRGINIA 23529

METHODOLOGY FOR SENSITIVITY ANALYSIS, APPROXIMATE ANALYSIS, AND DESIGN OPTIMIZATION IN CFD FOR MULTIDISCIPLINARY APPLICATIONS

By

Arthur C. Taylor III, Principal Investigator
Gene W. Hou, Co-Principal Investigator

Progress Report
For the period April 15, 1991 to April 14, 1992

April 1992

Overview

This progress report for grant, NAG-1–1265, is given in the form of a manuscript which is currently under review for publication in the International Journal For Numerical Methods In Fluids, titled "Sensitivity Analysis, Approximate Analysis, and Design Optimization For Internal and External Viscous Flows," by Arthur C. Taylor, III, Gene W. Hou, and Vamshi Mohan Korivi. The manuscript was also presented as unpublished AIAA paper 91–3083 at the AIAA Aircraft Design Conference in Baltimore, MD, in September, 1991. The work illustrates the successful completion of all the tasks which were promised in the first year of the grant.

Dr. Arthur C. Taylor III
Assistant Professor

Sensitivity Analysis, Approximate Analysis, and Design Optimization For Internal and External Viscous Flows

Arthur C. Taylor III
Assistant Professor

Gene W. Hou
Associate Professor

Vamshi Mohan Korivi
Graduate Research Assistant

Department of Mechanical Engineering and Mechanics
Old Dominion University
Norfolk, Virginia 23529–0247

1

Sensitivity Analysis, Approximate Analysis, and Design Optimization For Internal and External Viscous Flows

Arthur C. Taylor III
Assistant Professor

Gene W. Hou
Associate Professor

Vamshi Mohan Korivi
Graduate Research Assistant

Department of Mechanical Engineering and Mechanics
Old Dominion University
Norfolk, Virginia 23529–0247

ABSTRACT

Fundamental equations of aerodynamic sensitivity analysis and approximate analysis for the 2D thin-layer Navier-Stokes equations are reviewed. and special boundary condition considerations necessary to apply these equations to isolated lifting airfoils on "C" and "O" meshes are discussed in detail. An efficient strategy which is based on the finite element method and an elastic membrane representation of the computational domain is successfully tested, which circumvents the costly "brute force" method of obtaining grid sensitivity derivatives, and is also useful in mesh regeneration. The issue of turbulence modeling is addressed in a preliminary study. Aerodynamic shape sensitivity derivatives are efficiently calculated, and their accuracy is validated on two viscous test problems, including: 1) internal flow through a double-throat nozzle, and 2) external flow over a NACA 4-digit airfoil. An automated aerodynamic design optimization strategy is outlined which includes the use of a design optimization program, an aerodynamic flow analysis code, an aerodynamic sensitivity and approximate analysis code, and a mesh regeneration and grid sensitivity analysis code. Application of the optimization methodology to the two test problems in each case resulted in a new design having a significantly improved performance in the aerodynamic response of interest.

1.0 Introduction

The focus of the present study is the continued development of efficient techniques for computing aerodynamic sensitivity derivatives for steady, viscous internal and external flows (Ref. [1]). In particular, this present work involves a direct extension of the recently developed methods of Refs. [2] through [7], which have been successfully demonstrated on inviscid and viscous internal channel flows, to the classic external flow problem of an isolated airfoil. This extension to external flows is in essence a boundary condition problem.

Sensitivity derivatives are defined as the derivatives of the system responses of interest (e.g., the specific thrust (F_s) of a nozzle, or the lift (C_L), drag (C_D), and pitching moment (C_M) coefficients of an airfoil) taken with respect to the design variables of interest (e.g., the parameters which define the geometric shape of the system, such as the thickness and camber of an airfoil). Once computed, these sensitivity derivatives are potentially useful in many ways. For example, the sensitivity derivatives can be used in approximate analysis, where if the changes in the design variables are small, resulting changes in a system's response(s) can be accurately estimated, resulting in significant savings in computational costs. In addition, one of the most important applications of sensitivity derivatives is in engineering design optimization. The use of sensitivity derivatives in aerodynamic design optimization is demonstrated in the test problems to be presented.

The present study is therefore design oriented, with the ultimate goal of the work being the development of tools which can be used by design engineers together with modern CFD (Computational Fluid Dynamics) software in improving the aerodynamic performance of the systems to which these codes are applied. Recent research efforts in the subject of aerodynamic sensitivity analysis with applications to design optimization have been intensive, and Refs. [8] through [20] is a representative (but not exhaustive) list of closely related works by other researchers, given here to provide additional background material on the subject, and its status.

The remainder of the work is organized as follows: After the introduction, the next section is a presentation of theory, a section which is further sub-divided into six sub-sections, including 1)

3

governing equations, 2) spatial discretization and implicit formulation, 3) fundamental equations of sensitivity analysis and approximate analysis, 4) boundary conditions, 5) grid sensitivity, and 6) ancillary sensitivity relationships. In the next section, the computational results are given in application to two test problems, including an internal flow through a double-throat nozzle, and an external flow over a NACA 4-digit airfoil. The final major section is a summary of the work where conclusions are given.

2.0 Presentation of Theory

2.1 Governing Equations

The governing equations in this study are the 2-D thin-layer Navier-Stokes equations, given as:

$$\frac{1}{J}\frac{\partial Q}{\partial t} = R(Q) \tag{1}$$

where:

$$R(Q) = -\frac{\partial \hat{F}(Q)}{\partial \xi} - \frac{\partial \hat{G}(Q)}{\partial \eta} + \frac{\partial \hat{G}_v^{tl}(Q)}{\partial \eta} \tag{2}$$

$$Q = [\rho, \ \rho u, \ \rho v, \ \rho e_0]^T \tag{3}$$

R(Q) is called the residual, and is clearly equal to zero for a steady-state solution. Q is a vector of conserved variables, ρ is density, u and v are velocity components in Cartesian coordinates, and e_0 is total energy (i.e., $e_0 = e + \frac{u^2 + v^2}{2}$, where e is the specific internal energy of the fluid). The inviscid flux vectors, $\hat{F}(Q)$ and $\hat{G}(Q)$ are given by:

$$\hat{F}(Q) = \frac{\xi_x}{J}F(Q) + \frac{\xi_y}{J}G(Q)$$
$$\hat{G}(Q) = \frac{\eta_x}{J}F(Q) + \frac{\eta_y}{J}G(Q) \tag{4}$$

A transformation to generalized (ξ, η) coordinates from Cartesian (x,y) coordinates has been made in Eq. (1), where $\xi_x, \xi_y, \eta_x, \eta_y$ are metric terms, and J is the determinant of the Jacobian matrix of this transformation. The Cartesian flux vectors F(Q) and G(Q) are given by:

$$F(Q) = \left[\rho u, \; \rho u^2 + P, \; \rho uv, \; (\rho e_0 + P)u\right]^T$$

$$G(Q) = \left[\rho v, \; \rho uv, \; \rho v^2 + P, \; (\rho e_0 + P)v\right]^T$$

(5)

The pressure, P, is evaluated using the ideal gas law:

$$P = (\gamma - 1)\left[\rho e_0 - \rho\left(\frac{u^2 + v^2}{2}\right)\right]$$

(6)

and γ is the ratio of specific heats, taken to be 1.4. The thin-layer viscous terms in generalized coordinates are given by:

$$\hat{G}_v^{tl}(Q) = \left(\frac{\mu}{Re_L}\right)[\hat{g}_{v_1}, \hat{g}_{v_2}, \hat{g}_{v_3}, \hat{g}_{v_4}]^T$$

(7)

where:

$$\hat{g}_{v_1} = 0$$

$$\hat{g}_{v_2} = \alpha_1 u_\eta + \alpha_3 v_\eta$$

$$\hat{g}_{v_3} = \alpha_3 u_\eta + \alpha_2 v_\eta$$

$$\hat{g}_{v_4} = \frac{1}{2}\alpha_1(u^2)_\eta + \frac{1}{2}\alpha_2(v^2)_\eta$$

$$+ \alpha_3(uv)_\eta + \frac{\alpha_4}{Pr(\gamma - 1)}(a^2)_\eta$$

(8)

$$\alpha_1 = \left(\frac{\eta_y^2}{J} + \frac{4}{3}\frac{\eta_x^2}{J}\right), \quad \alpha_2 = \left(\frac{\eta_x^2}{J} + \frac{4}{3}\frac{\eta_y^2}{J}\right),$$

$$\alpha_3 = \left(\frac{1}{3}\frac{\eta_x \eta_y}{J}\right), \quad \alpha_4 = \frac{\eta_x^2 + \eta_y^2}{J}$$

The molecular viscosity is given by μ, Stokes' hypothesis for the bulk viscosity ($\lambda = -2\mu/3$) has been used, a is the speed of sound, Pr is the Prandtl number (taken to be 0.72), and Re_L is the Reynolds number. Nondimensionalization of Eq. (1) is with respect to ρ_∞ and U_∞, the freestream density and velocity, respectively. The physical coordinates (x,y) are nondimensionalized by a reference length, L, and the viscosity is nondimensionalized by μ_∞, the

5

molecular viscosity of the freestream. The nondimensional molecular viscosity can be computed using Sutherland's law and a reference temperature, T_∞, the static temperature of the freestream. For additional simplicity, however, in the laminar flow calculations of this work, the molecular viscosity is taken to be constant, equal to that of the freestream. For turbulent flow calculations, the algebraic turbulence model of Baldwin and Lomax [21] is used.

2.2 Spatial Discretization and Implicit Formulation

The governing equations are solved in their alternative integral conservation law form using an upwind cell-centered finite volume formulation. Only an overview of this method is presented here, with additional details found in Refs. [22] through [28]. With this approach, the residual at each cell becomes a balance of inviscid and viscous fluxes across cell interfaces. As an example, this flux balance for the jk^{th} cell in a typical computational grid is given by Eq. (9), for a steady–state solution, and for $\Delta\xi = \Delta\eta = 1$

$$-R_{jk} = \hat{F}_{j+\frac{1}{2}} - \hat{F}_{j-\frac{1}{2}} + \hat{G}_{k+\frac{1}{2}} - \hat{G}_{k-\frac{1}{2}} - \hat{G}^{tl}_{v_{k+\frac{1}{2}}} + \hat{G}^{tl}_{v_{k-\frac{1}{2}}} = 0 \tag{9}$$

where subscripts j,k in Eq. (9) refer to the ξ,η directions, respectively, and subscripts $j \pm \frac{1}{2}$ refer to the ξ = constant cell interfaces of the jk^{th} cell, subscripts $k \pm \frac{1}{2}$ refer to the η = constant cell interfaces of the jk^{th} cell. (All references to quantities which are evaluated at the cell interfaces will therefore require only a single subscript, either $j \pm \frac{1}{2}$ or $k \pm \frac{1}{2}$.) R_{jk} is the discrete representation of the residual at the jk^{th} cell. Upwind evaluation of the inviscid fluxes is accomplished by upwind interpolation of the field variables, Q, from the approximate cell centers to the cell interfaces, where the flux vector splitting procedure of van Leer [29] is employed. A third-order accurate upwind biased inviscid flux balance is used in the streamwise (ξ) and in the normal (η) directions. The finite volume equivalent of second-order accurate central differences is used for the viscous terms. The resulting discrete higher-order accurate algebraic approximate representation of the residual at each cell depends locally on cell-centered values of the vector Q at nine cells. That is, for the jk^{th} interior cell

$$R_{jk}(Q) = R_{jk}(Q_{j,k}, Q_{j,k-1}, Q_{j,k+1}, Q_{j,k-2}, Q_{j,k+2}, Q_{j-1,k}, Q_{j+1,k}, Q_{j-2,k}, Q_{j+2,k}) \tag{10}$$

Clearly adjustments are needed to Eq. (10) for interior cell equations which are adjacent to the boundaries. When written for each cell (including boundary condition relationships to be discussed) and assembled globally, this can be expressed as

$$\{R(Q^*)\} = \{0\} \tag{11}$$

where $\{Q^*\}$ is called the "root" (i.e., the steady-state value of the field variables). Therefore, Eq. (11) represents a large coupled system of nonlinear algebraic equations, and thus finding a steady-state solution to the governing equations has been replaced (approximately) by the problem of finding the root, $\{Q^*\}$, of this set of algebraic equations.

The governing equations are discretized in time using the Euler implicit method, followed by a Taylor's series linearization of the discrete equations about the known time level. This results in a large system of linear equations at each time step, given as

$$\left(\left[\frac{1}{J\Delta t}\right] - \left[\frac{\partial R^n(Q)}{\partial Q}\right]\right)\{^n\Delta Q\} = R^n(Q) \tag{12}$$

$$\{Q^{n+1}\} = \{Q^n\} + \{^n\Delta Q\}$$
$$n = 1, 2, 3, \ldots \tag{13}$$

Equations (12) and (13) represent the fundamental implicit formulation for integrating the governing equations in time to steady-state. In these equations, n is the time iteration index, and $\{^n\Delta Q\}$ is the incremental change in the field variables between the known (n^{th}) and the next ($n+1^{th}$) time levels. The matrix, $\left[\frac{1}{J\Delta t}\right]$, is diagonal, and contains the time term.

In constructing exactly the true global Jacobian matrix, $\left[\frac{\partial R^n(Q)}{\partial Q}\right]$, of Eq. (12), both the interior cell equations as well as the boundary conditions must be considered, (although the contributions to this matrix from the boundary condition equations are typically neglected in many CFD codes). Considering the contribution to this Jacobian matrix from interior cell

7

equations only, the four component vector equation which is associated with the jk^{th} interior cell is isolated and extracted from the global linear system, Eq. (12), and is written below as

$$[A]\{^n\triangle Q_{j,k-1}\} + [B]\{^n\triangle Q_{j,k}\} + [C]\{^n\triangle Q_{j,k+1}\} + [D]\{^n\triangle Q_{j,k-2}\} + [E]\{^n\triangle Q_{j,k+2}\} +$$

$$[F]\{^n\triangle Q_{j-1,k}\} + [G]\{^n\triangle Q_{j+1,k}\} + [H]\{^n\triangle Q_{j-2,k}\} + [I]\{^n\triangle Q_{j+2,k}\} = \{R^n_{jk}(Q)\} \qquad (14)$$

where $\{R^n_{jk}(Q)\}$ is given by Eq. (10), and of course Eq. (14) represents the linearized form of Eq. (10). The nine-point "difference stencil" represented by Eq. (14) is illustrated in Fig. (1), for a typical interior cell. The nine 4x4 coefficient matrices [A] through [I] of Eq. (14) are constructed of linear combination of the inviscid and viscous flux Jacobian matrices, and [B] also includes the time term.

As a consequence of Eq. (14), following global assembly of all interior cell equations, the resulting global coefficient matrix of Eq. (12) is sparse and has a banded structure, with nine non-zero diagonals, the individual elements of which are 4x4 block matrices. This matrix structure is illustrated in Fig. (2), which was taken from Ref. [30]. Note that consistent implicit treatment of the boundary condition equations and inclusion of these terms in the global coefficient matrix will sometimes severely disrupt the matrix structure which is illustrated in Fig. (2), depending of course on the type of boundary conditions. In addition to its use in Eq. (12) for time integration of the governing equations, this important Jacobian matrix, $\left[\frac{\partial R^n(Q)}{\partial Q}\right]$, plays another central role in this study, which will be shown later.

In principle, Eq. (12) can be repeatedly solved directly (using Eq. (13) to update the field variables), as the solution is advanced in time to steady-state, and for very large time steps, the direct method represents Newton's root finding procedure for nonlinear equations [31,32,33]. The direct method however is not necessarily the most efficient procedure with respect to overall CPU time, and the large storage requirements of the method make its use not feasible in 3D. Therefore, more commonly, an iterative algorithm is selected for use in the repeated solution of Eq. (12). Popular choices of these iterative algorithms include approximate factorization (AF) [34], conventional relaxation algorithms [26,27,35], the strongly implicit procedure (SIP)

[36], and the preconditioned conjugate gradient method [37,38], to name a few. In the present research, the AF algorithm is used in the test problems to obtain steady-state numerical solutions to the governing equations.

2.3 Fundamental Equations For Approximate Analysis and Sensitivity Analysis

In this section, fundamental equations of aerodynamic sensitivity analysis and approximate analysis are reviewed, with additional details given in Refs. [1] through [7]. Consider the vector, $\vec{\beta}$, the elements of which are independent variables which are typically called the design variables. Some, none, or all of the variables may be related to the geometric shape of the flow problem of interest, although the emphasis of the present study will be that of geometric shape variation. Computationally, the geometric shape of the domain is defined by the mesh upon which calculations are made, and the complete vector of (x,y) coordinates which defines the mesh is represented here symbolically as $\{\bar{X}\}$. For a steady-state solution, the discrete residual vector given by Eq. (11) is rewritten in the following form

$$\{R(Q^*(\vec{\beta}), \bar{X}(\vec{\beta}), \vec{\beta})\} = \{0\} \tag{15}$$

where in the above, the direct dependence of the residual on the computational mesh, $\{\bar{X}\}$, as well as its direct dependence (if any) on the vector $\vec{\beta}$ is now emphasized explicitly. Direct differentiation of Eq. (15) with respect to β_k, the kth element of $\vec{\beta}$, yields

$$-\left[\frac{\partial R}{\partial Q}\right]\left\{\frac{\partial Q^*}{\partial \beta_k}\right\} = \left[\frac{\partial R}{\partial \bar{X}}\right]\left\{\frac{\partial \bar{X}}{\partial \beta_k}\right\} + \left\{\frac{\partial R}{\partial \beta_k}\right\} \tag{16}$$

$$\text{Term 1} \qquad\qquad \text{Term 2} \qquad \text{Term 3}$$

Equation (16) is an exact derivative of the discrete algebraic residual vector, and represents the central and most general relationship upon which those which follow in this section are based. The Jacobian matrix, $\left[\frac{\partial R}{\partial Q}\right]$, of Term 1 of Eq. (16) is identical to that found in the fundamental implicit formulation for time integration (Eq. (12)), and is evaluated here at the steady-state solution. It is thus well understood. The solution vector, $\left\{\frac{\partial Q^*}{\partial \beta_k}\right\}$, is the sensitivity of the complete vector of field variables with respect to the kth design variable. The matrix,

9

$\left[\frac{\partial R}{\partial X}\right]$, of Term 2 is the Jacobian of the steady-state discrete residual vector with derivatives taken with respect to the complete vector of (x,y) grid coordinates, and is documented in Refs. [3,5]. The vector, $\left\{\frac{\partial \bar{X}}{\partial \beta_k}\right\}$, of Term 2 contains what is known here as the grid sensitivity terms, and is discussed in greater detail in Ref. [4], and also will be given special consideration later in the present study. The vector, $\left\{\frac{\partial R}{\partial \beta_k}\right\}$, (Term 3) accounts for derivatives resulting from direct dependencies (if any) of the residual vector on β_k.

In the event that β_k is not a geometric shape related design parameter (e.g., the back pressure in a subsonic nozzle, or the angle of attack (α) or freestream Mach number (M_∞) for a airfoil) then Term 2 of Eq. (16) will be zero. If β_k is a geometric shape design parameter, its entire effect on the residual will typically be felt through the grid, and Term 3 of Eq. (16) will generally be zero. Therefore, Eq. (16) becomes

$$-\left[\frac{\partial R}{\partial Q}\right]\left\{\frac{\partial Q^*}{\partial \beta_k}\right\} = \left\{\frac{\partial R}{\partial \beta_k}\right\} \tag{17}$$

when variation of geometric shape is not involved, and becomes

$$-\left[\frac{\partial R}{\partial Q}\right]\left\{\frac{\partial Q^*}{\partial \beta_k}\right\} = \left[\frac{\partial R}{\partial \bar{X}}\right]\left\{\frac{\partial \bar{X}}{\partial \beta_k}\right\} \tag{18}$$

when β_k is a geometric shape design parameter. Eq. (18) represents the central relationship which is successfully demonstrated in Ref. [4] for accurately computing aerodynamic sensitivity derivatives with respect to variation of geometric shape.

An approximate version of Eq. (18) which is useful in approximate analysis for estimating the steady-state solution changes which occur in response to small but finite geometric shape variations is given by

$$-\left[\frac{\partial R}{\partial Q}\right]\{\Delta Q^*\} \approx \left[\frac{\partial R}{\partial \bar{X}}\right]\{\Delta \bar{X}\} \tag{19}$$

where the approach represented by Eq. (19) is studied in detail in Refs. [3] and [5] for internal inviscid and viscous flows, respectively. In developing approximate analysis methods, other approaches of interest which might be used are

$$-\left[\frac{\partial R}{\partial Q}\right]\{\Delta Q^*\} \approx \left\{\frac{\partial R}{\partial \beta_k}\right\}\Delta \beta_k \tag{20}$$

for variations other than geometric shape, (which is an approximate version of Eq. (17)), and

$$-\left[\frac{\partial R}{\partial Q}\right]\{\Delta Q^*\} \approx \left[\frac{\partial R}{\partial X}\right]\left\{\frac{\partial X}{\partial \beta_k}\right\}\Delta\beta_k \qquad (21)$$

for geometric shape variations only (which is a minor variation of Eq. (19)).

In a typical design sensitivity analysis, the solution vector, $\left\{\frac{\partial Q^*}{\partial \beta_k}\right\}$, of the preceding equations will provide far more information than is actually sought, and only a relatively small subset of this vector is extracted for use. For example, if the sensitivity derivatives of the aerodynamic forces on a solid surface boundary are to be calculated for a viscous flow, then the sensitivity derivatives of the surface pressures and velocity gradients at the wall will be needed, which can be obtained as a subset of $\left\{\frac{\partial Q^*}{\partial \beta_k}\right\}$. This is explained more fully in a subsequent sub-section, where the ancillary sensitivity equations of specific use herein are presented.

2.4 Boundary Conditions

In the implementation of the fundamental equations of aerodynamic sensitivity analysis and approximate analysis, which were reviewed in the previous sub-section (Eqs. (15) through (21)), the consistent treatment and inclusion of the boundary conditions in these equations is essential, and must not be considered optional, as it typically is in the integration of the equations in time (Eq. (12)). The severely erroneous results which can arise as a consequence of failure to properly treat the boundary conditions are illustrated in an example problem in Ref. [2], with additional documentation on boundary condition treatment given in Ref. [6].

For the isolated lifting airfoil problem, where the governing equations are typically solved on "C" or "O" meshes, the consistent treatment of the boundary conditions (during sensitivity analysis) is considerably more involved than that which is typically encountered in handling the boundary conditions for standard internal flow problems. Therefore, the objective of this section is to describe these difficulties, and to discuss various remedies. Many of the ideas to be presented in this section are taken from Refs. [33,39] involving the use of Newton (direct) solvers in obtaining inviscid and viscous steady-state solutions to airfoil problems.

11

2.4.1 Airfoil Surface Boundary Conditions

The consistent treatment of the boundary conditions which are applied on the surface of the airfoil in this study (i.e., standard no-slip conditions) does not present any additional difficulty beyond that which is encountered for the boundary conditions which are used in typical internal flow problems. That is, the explicit application of the airfoil surface boundary conditions (as well as the application of all boundary conditions which are used in the internal flow problem to be presented) can be represented at each point where the boundary conditions are applied (i.e., at the boundary cell faces in the present study) as the solution of a boundary condition residual equation of the form given by

$$\{ R_B(Q_B^*(\vec{\beta}), Q_I^*(\vec{\beta}), \bar{X}_I(\vec{\beta}), \vec{\beta}) \} = \{0\} \tag{22}$$

where $\{R_B\}$ is a nonlinear <u>four component</u> vector function of (at most) the local field variables, Q_B^*, at the boundary cell face, Q_I^*, the local field variables at the first interior cell adjacent to the boundary, $\bar{X}_I$, the local coordinates of the grid, and also the very likely possibility of an explicit dependence on $\vec{\beta}$ is included. Differentiation with respect to β_k, the kth design variable, yields

$$-\left[\frac{\partial R_B}{\partial Q_B}\right]\left\{\frac{\partial Q_B^*}{\partial \beta_k}\right\} - \left[\frac{\partial R_B}{\partial Q_I}\right]\left\{\frac{\partial Q_I^*}{\partial \beta_k}\right\} = \left\{\frac{\partial R_B}{\partial \beta_k}\right\} \tag{23}$$

when geometric shape is not involved, and

$$-\left[\frac{\partial R_B}{\partial Q_B}\right]\left\{\frac{\partial Q_B^*}{\partial \beta_k}\right\} - \left[\frac{\partial R_B}{\partial Q_I}\right]\left\{\frac{\partial Q_I^*}{\partial \beta_k}\right\} = \left[\frac{\partial R_B}{\partial \bar{X}_I}\right]\left\{\frac{\partial \bar{X}_I}{\partial \beta_k}\right\} \tag{24}$$

when geometric shape variables are involved. For approximate analysis, Eq. (23) can be written as

$$-\left[\frac{\partial R_B}{\partial Q_B}\right]\{\Delta Q_B^*\} - \left[\frac{\partial R_B}{\partial Q_I}\right]\{\Delta Q_I^*\} \approx \left\{\frac{\partial R_B}{\partial \beta_k}\right\}\Delta\beta_k \tag{25}$$

if geometric shape is not involved, and Eq. (24) can be written as either of the following two equations

$$-\left[\frac{\partial R_B}{\partial Q_B}\right]\{\Delta Q_B^*\} - \left[\frac{\partial R_B}{\partial Q_I}\right]\{\Delta Q_I^*\} \approx \left[\frac{\partial R_B}{\partial \bar{X}_I}\right]\{\Delta \bar{X}_I\} \tag{26}$$

$$-\left[\frac{\partial R_B}{\partial Q_B}\right]\{\Delta Q_B^*\} - \left[\frac{\partial R_B}{\partial Q_I}\right]\{\Delta Q_I^*\} \approx \left[\frac{\partial R_B}{\partial \bar{X}_I}\right]\left\{\frac{\partial \bar{X}}{\partial \beta_k}\right\}\Delta\beta_k \tag{27}$$

for predictions of geometric shape change.

Equations (23), (24), (25), (26), and (27) are of course fully a part of the global linear systems of equations given by Eqs. (17), (18), (20), (19) and (21), respectively, and can be explicitly included and solved simultaneously with the interior cell equations during the solution of these linear systems. Alternatively, yet equivalently, these boundary conditions equations can be pre-eliminated (i.e., pre-solved and substituted into the remaining interior cell equations) prior to simultaneous solution of the global linear systems. Pre-elimination of the boundary condition equations is the approach selected in the present study, and is explained in greater detail in Ref. [2]. Note that in general, contributions to the Jacobian matrix, $\left[\frac{\partial R}{\partial X}\right]$, of the right-hand sides of Eqs. (16), (18), (19) and (21) can also occur (for some boundary condition types) from these boundary condition equations (in addition of course to the contributions to the matrix, $\left[\frac{\partial R}{\partial Q}\right]$).

It is significant to note that simple boundary conditions of the form given by Eq. (22) result in consistently linearized boundary condition equations (i.e., Eqs. (23) through (27)) which, when included, do not in any way alter the basic structure of the coefficient matrix $\left[\frac{\partial R}{\partial Q}\right]$, illustrated in Fig. (2) (i.e., the nine-diagonal, 4x4 block structure is preserved exactly), and thus direct solution of the fundamental systems of equations of sensitivity analysis and approximate analysis is not further complicated by inclusion of these boundary conditions equations. Unfortunately however, this is not the case in general, for all boundary condition types, as will be seen subsequently.

2.4.2 Periodic Boundary Conditions For "C" and "O" Meshes

When calculating flows over airfoils, in the likely event that a "C" or "O" type mesh has been selected for the calculations, "periodic" boundary conditions are applied along the "wake cut" of the computational grid. There are different ways that these periodic boundary conditions could be applied. In the present research, the explicit application of these boundary conditions is not expressed (as before) as the solution of special boundary condition equations of the type given by Eq. (22). Instead, interior cell residual equations for the interior cells immediately adjacent to the "periodic" boundaries (i.e., the wake–cut) are each expressed as functions of cell-centered values of the vector Q at nine cells in the domain (i.e., for a higher-order accurate

13

upwind spatial discretization), where this functional relationship in <u>physical space</u> is identical to that expressed by Eq. (10) for a general interior cell. This means that wherever necessary, the evaluation of the inviscid flux vectors of Eq. (9) is accomplished by a consistent upwind interpolation of the field variables from local interior cells across the wake cut, and that the terms of the viscous flux vectors are evaluated using consistent central differences across the wake cut.

Although the functional relationship expressed by Eq. (10) for a general interior cell equation is preserved in physical space for interior cells involving periodic boundary conditions, clearly it is <u>not</u> preserved for these cells (with respect to the structure and ordering of the cells) in the <u>computational</u> domain. That is, when periodicity is involved, the interior cell equations depend explicitly on the field variables at local neighboring cells in the computational grid, and in addition, become functionally dependent on the field variables of cells which are quite distant in the computational ordering. Consequently, the linearized version of Eq. (10), given by Eq. (14) for a general interior cell, must be modified for interior cells involving periodicity, in order to properly account for these boundary conditions. Periodic boundary conditions affect each first and second interior cell equation immediately adjacent to the boundary where "periodicity" is enforced, resulting (for the higher-order spatial discretization) in two periodic 4x4 matrix terms contributing to the left-hand side of Eq. (14) for the first interior cell equation, and one such periodic term for the second interior cell equation.

The most significant impact of the periodic boundary conditions is that there is some restructuring of the coefficient matrix, $\left[\frac{\partial R}{\partial Q}\right]$, where the neat, banded, nine-diagonal structure which is illustrated in Fig. (2) is no longer preserved exactly. This is illustrated in Ref. [33], and is of course is a consequence of the previously discussed adjustments to Eq. (14) which are required for the interior cell equations involving periodicity. Furthermore, depending on the direction which is selected when ordering sequentially the individual cell equations for assembly into the global linear system (either the tangential (J) to the airfoil direction, or the normal (K) to the airfoil direction), the non-zero contributions to the global coefficient matrix from the periodic boundary conditions will fall either inside or outside of the central bandwidth of the matrix. (Note: The <u>central</u> bandwidth here refers to all of the matrix elements, either zero

14

or non-zero, which fall between the outermost diagonals, [H] and [I], of Fig. (2) and is thus the bandwidth of the matrix, neglecting periodic terms, if any, which fall outside.) For "C" or "O" mesh calculations, if the equations are numbered in the tangential (J) direction, the periodic coefficients will all fall inside the central bandwidth, but will all fall outside the central bandwidth (some at extreme distances) if the numbering is in the normal (K) direction. (Exception: There exists a special method explained in Ref. [33] for numbering the equations in the "K" direction for "C" meshes where the periodic coefficients all fall completely inside the central bandwidth. This method results in a doubling of the central bandwidth of that which is achieved with a standard "K" ordering of the equations, and hence this non-standard ordering was rejected in the present study).

A "J" direction ordering of the equations will therefore in principle allow the use of a pure banded matrix direct solver solution procedure which takes advantage of the fact (in terms of storage and work) that outside of the central bandwidth, all of the matrix elements are zero. In contrast, for a pure direct solution of the linear system, a standard "K" direction ordering will require the use of a full matrix solver to account for the periodic terms, which is not feasible for practical fluids problems involving the full governing equations, even in 2D.

For typical airfoil calculations, the "J" dimension of the grid is usually significantly larger than the "K" dimension. A standard "K" ordering of the equations will thus result in a significantly smaller central bandwidth of the coefficient matrix than will a "J" ordering. To overcome this dilemma, a hybrid direct solver / conventional Richardson type relaxation strategy is proposed and implemented in the present study, for airfoil problems on "C" and "O" meshes, as follows:

1) A "K" direction (i.e., normal to the airfoil) numbering of the equations is used in constructing the coefficient matrix, $\left[\frac{\partial R}{\partial Q}\right]$, in order to minimize the width of the central bandwidth.

2) The coefficient matrix is split into two parts, such that

$$-\left[\frac{\partial R}{\partial Q}\right] = [M] + [N] \tag{28}$$

15

where the matrix [M] contains all of the elements which fall inside of the central bandwidth of $\left[\frac{\partial R}{\partial Q}\right]$. Thus [M] has the matrix structure illustrated in Fig. (2). The matrix [N] is thus very sparse, and contains all of the non-zero contributions to $\left[\frac{\partial R}{\partial Q}\right]$ which fall outside the central bandwidth, resulting from the periodic boundary conditions.

3) The matrix [M] is LU factored directly using a conventional banded matrix solver, to yield

$$[M] = [L][U] \tag{29}$$

4) A conventional Richardson type iterative strategy is invoked which in principle could be applied to Eqs. (16), (17), (18), (19), (20), and/or (21). For example, if Eq. (18) is selected, the iterative strategy is

$$[L][U]\left\{\frac{\partial Q^*}{\partial \beta_k}\right\}^i = \left[\frac{\partial R}{\partial X}\right]\left\{\frac{\partial \bar{X}}{\partial \beta_k}\right\} - [N]\left\{\frac{\partial Q^*}{\partial \beta_k}\right\}^{i-1}$$

$$i = 1,2,3,\cdots,(\,imax)^k \tag{30}$$

$$k = 1, ndv$$

where in the above, 'i' is the innermost index, $(imax)^k$ is the maximum number of iterations required to converge the kth linear system to the desired tolerance, 'k' is the outermost index, which associates the solution vector, $\left\{\frac{\partial Q^*}{\partial \beta_k}\right\}^{(imax)^k}$ with a particular k^{th} design variable, and ndv is the total number of design variables for which sensitivity derivatives are required. It is emphasized that since [L] and [U] (in addition to $\left[\frac{\partial R}{\partial X}\right]$ and [N]) are constant with respect to the indices 'i' and 'k', they only need be computed once and repeatedly reused. Following the LU factorization, a single iteration of Eq. (30) is inexpensive, of course, since [L] and [U] are lower and upper triangular matrices, respectively.

The coefficient matrix, $\left[\frac{\partial R}{\partial Q}\right]$, is diagonally dominant for a first order upwind spatial discretization, but is not diagonally dominant for a higher-order spatial discretization [26], and therefore, convergence of the iterative strategy represented by Eqs. (28), (29) and (30) is not

assured [35]. In the airfoil test problem to be presented, the iterative strategy of Eq. (30) was at first divergent, but was subsequently made convergent through the simple use of a single conventional under-relaxation parameter, ω (omega). Other remedies which are suggested as possible methods to correct the failure of this iterative strategy to converge include, but are not limited to:

1) Use of a first order accurate upwind spatial discretization for the inviscid terms of the first row of interior cells immediately adjacent to the wake cut, which will result in only a single non-zero periodic 4x4 matrix coefficient contribution (instead of three such coefficients) to the matrix [N] of Eqs. (28) and (30), for each point where periodicity is enforced.

2) Use of a "ghost" cell equation at each point where periodicity is enforced, which is retained explicitly in the global coefficient matrix, resulting in a more strongly implicit treatment of the periodic terms, with complete preservation of higher-order accuracy across the wake cut. This is the approach of Ref. [33], where difficulties with convergence of the iterative strategy were not encountered [39].

3) Use of matrix pre-conditioning.

In addition to the contributions to the matrix, $\left[\frac{\partial R}{\partial Q}\right]$, resulting from the application of periodic boundary conditions, there are also contributions to the matrix, $\left[\frac{\partial R}{\partial X}\right]$, of Eqs. (16), (18), (19), and (21), which must be considered for <u>viscous</u> flow. For inviscid flow, there are no additional adjustments needed to $\left[\frac{\partial R}{\partial X}\right]$ to account for periodicity. However, a consistent treatment of all viscous metric terms in the application of periodic boundary conditions will result in the need for some adjustments to some of the terms of $\left[\frac{\partial R}{\partial X}\right]$ to properly account for the periodicity. A close examination of the documentation given in Ref. [5] on the details of the construction of the viscous terms of $\left[\frac{\partial R}{\partial X}\right]$ will provide additional explanation and verification of this.

2.4.3 Far-Field Boundary Conditions

The far-field boundary conditions which are used in this study make use of the Riemann invariants, and these boundary conditions are given in Refs. [33] and [40]. For lifting airfoils, it is well known that significantly improved computational accuracy can be achieved with the addition of a "point-vortex" correction to these boundary conditions. This "point-vortex" correction is developed and presented in detail in Ref. [40], and will be addressed in the context of its treatment in sensitivity analysis in this sub-section. If this point-vortex correction is $\underline{not}$ included, then the explicit application of the far-field boundary conditions at each location can be expressed exactly as the solution of a boundary condition residual expression of the form given previously by Eq. (22). In this event, the contribution from the far-field boundary conditions to the equations of sensitivity analysis and approximate analysis (i.e., to Eqs. (16) through (21)) is therefore very straightforward, using Eqs. (23) through (27).

The use of the "point-vortex" correction described in Ref. [40] to improve the far-field boundary conditions is straightforward to implement in an explicit sense. Its explicit implementation involves the use of a point-vortex (centered at the quarter chord) representation of the airfoil, where the strength of the point-vortex (i.e., the circulation, Γ) is proportional to the lift coefficient, C_L, of the airfoil. The purpose of this point-vortex is to more accurately model the influence of the lifting airfoil on the velocity field in the vicinity of the far-field boundaries, (compared to the alternative of assuming a freestream velocity field here), resulting in more accurate airfoil calculations, particularly as the extent of the far-field boundary from the airfoil is decreased.

The implementation of this point-vortex correction results in a numerical coupling between the far-field boundary condition equations and (through the lift coefficient, C_L) the field variables (and also the x,y grid coordinates) on and immediately adjacent to the surface of the airfoil. As a consequence of this coupling, there are algebraically messy, complex additions to the global Jacobian matrix, $\left[\frac{\partial R}{\partial Q}\right]$ (which destroy the banded matrix structure, illustrated in (Fig. (2)) and also to $\left[\frac{\partial R}{\partial X}\right]$. In order to avoid the task of explicitly deriving these terms and their precise

18

locations in these global Jacobian matrices, a simplifying strategy is proposed, which makes use of the following ideas:

1. In the discrete system of algebraic equations which models the steady-state fluid flow (i.e., Eq. (11)), the lift coefficient, C_L, is to be treated as an additional field variable.

2. The chain rule is employed judiciously.

3. In a typical sensitivity analysis for airfoil design, the sensitivity of the lift coefficient with respect to the design variables will be sought. Explicit expressions are therefore available for use in calculating the sensitivity derivatives of C_L with respect to the design variables, following solution of the global sensitivity equations. (This expression for C_L is given in a subsequent sub-section).

4. Recall that a strategy which involves <u>iteration</u> will be used to solve the equations of sensitivity and approximate analysis to account for the periodic boundary conditions (regardless of whether the point-vortex correction is used or not).

When the point-vortex correction is included, the boundary condition residual equation which is solved at each far-field boundary cell face can be expressed in a form similar to that of Eq. (22), except that an explicit dependence of the boundary condition equation on C_L is now identified. That is, Eq. (22) becomes:

$$\{R_B(Q_B^*(\vec{\beta}), Q_I^*(\vec{\beta}), \bar{X}_I(\vec{\beta}), \vec{\beta}, C_L)\} = \{0\} \tag{31}$$

where all the terms of Eq. (31) are as previously defined. Differentiation with respect to β_k, and applying the chain rule on the term involving C_L, the result is

$$-\left[\frac{\partial R_B}{\partial Q_B}\right]\left\{\frac{\partial Q_B^*}{\partial \beta_k}\right\} - \left[\frac{\partial R_B}{\partial Q_I}\right]\left\{\frac{\partial Q_I^*}{\partial \beta_k}\right\} = \left[\frac{\partial R_B}{\partial \bar{X}_I}\right]\left\{\frac{\partial \bar{X}_I}{\partial \beta_k}\right\} + \left\{\frac{\partial R_B}{\partial \beta_k}\right\} + \left\{\frac{\partial R_B}{\partial C_L}\right\}\frac{dC_L}{d\beta_k} \tag{32}$$

The four component vector, $\left\{\frac{\partial R_B}{\partial C_L}\right\}$, is very straightforward to derive analytically, since the explicit dependence of R_B on C_L is known and uncomplicated [40]. There are also additions to the matrix, $\left[\frac{\partial R_B}{\partial \bar{X}_I}\right]$, which are straightforward to derive, which arise as a consequence of this

boundary condition correction. The scalar term, $\frac{dC_L}{d\beta_k}$, is evaluated using an expression of the form

$$\frac{dC_L}{d\beta_k} = \left\{\frac{\partial C_L}{\partial Q}\right\}^T \left\{\frac{\partial Q^*}{\partial \beta_k}\right\} + \left\{\frac{\partial C_L}{\partial X}\right\}^T \left\{\frac{\partial \bar{X}}{\partial \beta_k}\right\} + \frac{\partial C_L}{\partial \beta_k} \tag{33}$$

where the global column vectors, $\left\{\frac{\partial C_L}{\partial Q}\right\}$ and $\left\{\frac{\partial C_L}{\partial X}\right\}$, are sparse. Since the value of $\frac{dC_L}{d\beta_k}$ is likely to be at least one of the desired final results of an airfoil sensitivity analysis, the precise terms involved in Eq. (33) (i.e., $\{\frac{\partial C_L}{\partial Q}\}^T$ and $\{\frac{\partial C_L}{\partial X}\}^T$) have been derived analytically for this purpose, and are given in a subsequent sub-section. Note in Eq. (33) that the notation for a total derivative has been used on the left-hand side of the equation, indicating that the <u>total</u> rate of change is included in the expression, and thus distinguishing it from the partial derivative (which accounts for explicit dependencies of C_L on β_k, if any) on the right-hand side of the equation. It should be understood, however, that $\frac{dC_L}{d\beta_k}$ is still a partial derivative in the sense that C_L is in general a function of multiple independent design variables.

Specialization of Eq. (32) to the case of either geometric or non-geometric shape design variables and to the case of either sensitivity analysis or approximate analysis is analogous to that shown in Eqs. (23) through (27). In particular, for approximate analysis, the term $\frac{dC_L}{d\beta_k}$ of Eq. (32) becomes ΔC_L, and Eq. (33) becomes:

$$\Delta C_L \approx \left\{\frac{\partial C_L}{\partial Q}\right\}^T \{\Delta Q^*\} + \left\{\frac{\partial C_L}{\partial X}\right\}^T \{\Delta \bar{X}\} + \frac{\partial C_L}{\partial \beta_k} \Delta \beta_k \tag{34}$$

At this point, the far-field boundary condition equations given by Eqs. (32) and (33) are in a convenient form for assembly into the global system of equations for subsequent solution in the hybrid direct solver / iterative strategy previously described, where iteration is also used to account for the periodic boundary condition terms (whether or not the point-vortex correction is included). Global assembly of Eq. (32) into the iterative strategy of Eq. (30) results in the following modified iteration strategy to account for the point-vortex correction

$$[L][U]\left\{\frac{\partial Q^*}{\partial \beta_k}\right\}^i = \left[\frac{\partial R}{\partial \bar{X}}\right]\left\{\frac{\partial \bar{X}}{\partial \beta_k}\right\} - [N]\left\{\frac{\partial Q^*}{\partial \beta_k}\right\}^{i-1} + \left\{\frac{\partial R}{\partial C_L}\right\}\frac{dC_L^{i-1}}{d\beta_k}$$
$$i = 1, 2, 3, \cdots, (\text{imax})^k \tag{35}$$
$$k = 1, \text{ndv}$$

where in Eq. (35) the only non-zero contributions to the global vector, $\left\{\frac{\partial R}{\partial C_L}\right\}$, are from the far-field point-vortex corrected boundary condition equations. The scalar term is repeatedly calculated for all 'i' and 'k' indices using the expression

$$\frac{dC_L^{\,i-1}}{d\beta_k} = \left\{\frac{\partial C_L}{\partial Q}\right\}^T \left\{\frac{\partial Q^*}{\partial \beta_k}\right\}^{i-1} + \left\{\frac{\partial C_L}{\partial X}\right\}^T \left\{\frac{\partial \bar{X}}{\partial \beta_k}\right\} + \frac{\partial C_L}{\partial \beta_k} \qquad (36)$$

The iterative strategy of Eq. (35) thus avoids the need for determining explicitly the algebraically messy contributions of the point-vortex corrected boundary conditions to the Jacobian matrices, $\left[\frac{\partial R}{\partial Q}\right]$ and $\left[\frac{\partial R}{\partial X}\right]$.

2.5 Mesh Sensitivity Analysis

In this section, calculation of the terms of the mesh sensitivity vector, $\left\{\frac{\partial \bar{X}}{\partial \beta_k}\right\}$, of Eqs. (16), (18), and (21) is given special consideration. One approach which can be used for calculation of these terms is the "brute force" finite difference method, where the geometric shape design parameters are perturbed slightly, one at a time, and the mesh generation program (which was used to generate the initial mesh) is repeatedly re-run to generate perturbed grids. Then, each grid sensitivity vector is calculated as

$$\left\{\frac{\partial \bar{X}}{\partial \beta_k}\right\} \approx \frac{\{\bar{X}(\beta_k + \Delta\beta_k)\} - \{\bar{X}(\beta_k - \Delta\beta_k)\}}{2\Delta\beta_k} \qquad (37)$$

where in the above, central finite difference approximations are used for greater accuracy, but require the generation of two perturbed meshes per design variable instead of the one which is required using a forward finite difference. The principle advantage of this approach is that it is conceptually simple and easily applied. For this reason, it is also well suited for use in an automated design optimization loop. Since by design the equations of mesh generation are typically very smooth, the method can be expected to be reliable in producing satisfactory accuracy. Furthermore, for simple 2D geometries using algebraic grid generation, the procedure should be computationally efficient, even when the number of design variables is large.

High quality elliptic and hyperbolic grid generation codes, which are often selected for generating "C" and "O" airfoil meshes, are far more computationally expensive to use than are

21

their algebraic counterparts, and thus use of the "brute force" method to obtain grid sensitivities in this case could become excessively costly, particularly if the number of design variables is large, and if the computations are to be made repeatedly in an automated design loop. One strategy proposed in Ref. [4] to help restore computational efficiency to this problem would be to differentiate analytically the equations of mesh generation (for the particular mesh generation code of choice), to determine the Jacobian matrix of the entire grid, $\bar{X}$, with respect to the grid points on the boundary of the domain, $\bar{X}_s$. Then grid sensitivity derivatives could be efficiently calculated using the relationship

$$\left\{ \frac{\partial \bar{X}}{\partial \beta_k} \right\} = \left[\frac{\partial \bar{X}}{\partial \bar{X}_s} \right] \left\{ \frac{\partial \bar{X}_s}{\partial \beta_k} \right\} \tag{38}$$

Other researchers [41] have implemented the approach of Eq. (38) in application to the airfoil grid generation program of Ref. [42]. Another important consideration with respect to some sophisticated grid generation codes is that they are used interactively, which would prohibit their use (interactively) in an automated design loop.

In order to help overcome these difficulties which have been discussed, a procedure is proposed herein for use in the repeated evaluation of grid sensitivity terms, as well as for use in efficient grid regeneration. The method, which will be presented subsequently, is based on an "elastic membrane" analogy to represent the computational domain, and grid sensitivity derivatives are calculated from a standard structural analysis computer program using the finite element method.

As the geometric shape of the flow domain is continuously changed, as required by any geometric shape optimization process, the mesh points in the domain must be properly adjusted in the design iterations, to avoid the numerical errors induced by excessive mesh distortion. The requirement of mesh regridding distinguishes shape design optimization from other design optimization applications. A simple way for automatic mesh regridding can be established by introducing a set of basic displacement vectors, $\bar{V}_k$, to describe the patterns by which the mesh is regridded. The relationship between the original mesh, $\bar{X}_o$, and the regridded one, $\bar{X}$, can

22

then be expressed in the form of a linear combination of these basic displacement vectors, and their associated weighting coefficients, β_k, as

$$\bar{X} = \bar{X}_o + \sum_{k=1}^{ndv} \beta_k \bar{V}_k \qquad (39)$$

where in the above, ndv is the number of design variables, if the weighting coefficients are taken to be the design variables. The vector, $\bar{X}_o$, represents the initial mesh, which is produced using any conventional mesh generation code of choice. In this case, the basic displacement vector, $\bar{V}_k$, is simply equal to the required mesh sensitivity vector, $\left\{ \frac{\partial \bar{X}}{\partial \beta_k} \right\}$, of Eqs. (16), (18), and (21). That is, the grid sensitivity derivatives are calculated by differentiation of Eq. (39), which yields

$$\left\{ \frac{\partial \bar{X}}{\partial \beta_k} \right\} = \{\bar{V}_k\} \qquad (40)$$

Note that the grid sensitivity vectors, $\{\bar{V}_k\}$, do not change when the design variables are changed, provided that the domain is always regridded using Eq. (39), as the shape of the domain changes. Therefore, these grid sensitivity derivatives need only be calculated once and then stored prior to the start of an aerodynamic optimization strategy, and they can be repeatedly re-used as often as needed for grid sensitivity analysis, as well as for automatic mesh regeneration.

The basic displacement vectors, $\bar{V}_k$, can be in any form; however, they must be independent of each other. In structural shape design optimization, the elastic displacements induced by the boundary perturbations are commonly selected to represent the basic displacement vectors. In this way, the movement of the mesh points is governed by the nature of linear elasticity, which not only preserves the continuity of the mesh, but also avoids any mesh-overlapping. It is proposed herein that the same practice can be applied to aerodynamic shape optimization problems, in which an imaginary elastic medium is introduced to represent the computational domain.

More specifically, the basic displacement vectors can be generated by either the fictitious load method [43], or the prescribed displacement method [44]. The former produces the basic displacement vectors by applying a unit load at each of the nodes along the boundary in the direction along which the node is allowed to move. This concept is illustrated in Fig. (3), for a representative airfoil grid. The latter, however, produces the basic displacement vectors by

imposing a non-zero displacement (in response to a unit change in each design variable) along the varied boundary. This concept is illustrated in Fig. (4), for a representative airfoil grid. The fictitious load method is usually applied to the case where the location of each node on the varied boundary is considered as a design variable, whereas the prescribed displacement method is good in the case where the shape of the boundary to be designed is parameterized.

In the following, a NACA 4-digit airfoil is employed as an example to demonstrate the application of the prescribed displacement method for mesh-regridding in an aerodynamic shape optimization environment. The profile of the NACA 4-digit airfoil can be precisely represented by polynomials in terms of the maximum thickness, T, the maximum camber, C, and the location of maximum camber, L, as

$$y(x) = \begin{cases} f(x) + C(2Lx - x^2)/L^2, & x \le L \\ f(x) + C(1 - 2L + 2Lx - x^2)/(1 - L)^2, & x > L \end{cases} \tag{41}$$

where

$$f(x) = \pm.5T(0.2969\sqrt{x} - 0.126x - 0.3516x^2 + 0.2843\,x^3 - 0.1015x^4) \tag{42}$$

where, the $\pm$ in the expression for f(x) is '+' for the upper surface of the airfoil, and '−' for the lower surface.

Since the derivatives of the airfoil shape with respect to T, C, and L are continuous, it is understood that small changes in T, C, and L will induce small changes in airfoil shape. Therefore, according to a Taylor's series expansion, such a change in the airfoil shape can be expanded approximately into a linear function of ΔT, ΔC, and ΔL, given as

$$y(x) = y_o(x) + \frac{\partial y_o(x)}{\partial T}\Delta T + \frac{\partial y_o(x)}{\partial C}\Delta C + \frac{\partial y_o(x)}{\partial L}\Delta L \tag{43}$$

where

$$\Delta T = T - T_o$$

$$\Delta C = C - C_o \tag{44}$$

$$\Delta L = L - L_o$$

where T_o, C_o, and L_o are the initial values of these three shape parameters associated with the initial airfoil shape, $y_o(x)$, and the initial grid, $\bar{X}_o$.

The derivatives $\frac{\partial y_o(x)}{\partial T}$, $\frac{\partial y_o(x)}{\partial C}$, and $\frac{\partial y_o(x)}{\partial L}$ in Eq. (43) represent special patterns which control the allowable changes in the airfoil's shape. The new mesh, $\bar{X}$ can be defined in a form given by Eq. (39) as

$$\bar{X} = \bar{X}_o + \Delta T \cdot \bar{V}_1 + \Delta C \cdot \bar{V}_2 + \Delta L \cdot \bar{V}_3 \qquad (45)$$

where ΔT, ΔC, and ΔL are taken to be the design variables (or equivalently T, C, and L are the design variables, through Eq. (44)). The basic displacement vectors, $\bar{V}_1$, $\bar{V}_2$, and $\bar{V}_3$ can be obtained by the prescribed displacement method, discussed above. These vectors are obtained numerically through implementation of a finite element model, with each cell in the computational mesh being considered as a plane stress quadrilateral element. A finite element matrix equation is formed to solve for each basic displacement vector (i.e., the movements of all the grid points) which is realized throughout the elastic membrane model of the domain, in response to the non-zero boundary movement which is specified through Eq. (43), for a unit change (or some other conveniently scaled change) in each of the design variables. Note that the finite element matrix equation is linear with a symmetric and banded coefficient matrix, which is solved directly by a single LU factorization, followed by multiple re-uses of this LU factorization as multiple solutions (i.e., one solution, $\bar{V}_k$, for each design variable) are obtained for multiple "load vectors" through simple efficient forward and backward substitutions.

It is clear that Eq. (43) represents a particular parameterization of the surface of the airfoil which will only closely approximately the NACA 4-digit parameterization defined by Eqs. (41) and (42) if ΔT, ΔC, and ΔL are small. However, if during design it is not a requirement to remain exactly within or close to the allowable shapes defined by the NACA 4-digit parameterization, then of course Eq. (43) is a valid (but different) parameterization of the airfoil shape, even for large ΔT, ΔC, and ΔL. Thus the classic NACA 4-digit airfoil is presented here only as an example.

In order to demonstrate and validate the mesh regeneration strategy, a numerical example is given. Starting with an extremely coarse initial grid, $\bar{X}_o$, with only 21x10 points (for illustration purposes), for a NACA 1412 airfoil (i.e., $T_o=0.12$, $C_o=0.01$, $L_o=0.40$), generated using the grid

25

generation code of Ref. [42], the domain was regridded using Eq. (45) for a new airfoil shape defined by Eq. (43) and (44), for C=0.04, T=T$_o$, and L=L$_o$. The initial airfoil and grid is shown in Fig. (5a), where in Fig. (5b), the new airfoil and grid are shown. The changes which are seen in the new mesh resulting from the application of this methodology appear satisfactory in this test example.

2.6 Ancillary Sensitivity Relationships

The purpose of this sub-section is to include some important extra terms and relationships which are used in the present study in computing sensitivity derivatives, in order to make the presentation of the methods more complete. Specifically, expressions are given for generalized aerodynamic force and moment coefficients in 2D, and their sensitivity derivatives. In addition, expressions are derived for use in computing the sensitivity derivatives of the thrust, mass flow rate, and specific thrust of a nozzle.

Fig. (6) illustrates the ith element (oriented at an arbitrary angle in space) which is located on the boundary of the geometric shape of interest, over / through which the fluid is passing. In the figure, the coordinates (x_{b_i}, y_{b_i}) and $(x_{b_{i+1}}, y_{b_{i+1}})$ are the physical (x,y) coordinates at either end of this ith element, and are assumed to be nondimensionalized by L, the reference length. The convention is established that as one moves along the surface in the direction of increasing the index, 'i', then the solid surface is on the right, and the fluid is on the left.

Nondimensional pressure (C_p) and skin friction (C_f) coefficients which are associated with this ith element on the boundary are defined as follows

$$C_{P_i} = \frac{P_{b_i}}{\frac{1}{2}\rho_\infty U_\infty^2} \qquad C_{f_i} = \frac{\tau_{b_i}}{\frac{1}{2}\rho_\infty U_\infty^2} \qquad (46)$$

where in the above, P_{b_i} and τ_{b_i} are the pressure and shear stress, respectively, which are associated with the ith element on the boundary, and $\frac{1}{2}\rho_\infty U_\infty^2$ is the dynamic pressure of the

freestream. Nondimensional force coefficients in the x and y directions, given as C_{x_i} and C_{y_i}, respectively, for the ith surface element, are given as

$$C_{x_i} = C_{p_i}\left(y_{b_{i+1}} - y_{b_i}\right) + C_{f_i}\left(x_{b_{i+1}} - x_{b_i}\right)$$
$$C_{y_i} = C_{p_i}\left(x_{b_i} - x_{b_{i+1}}\right) + C_{f_i}\left(y_{b_{i+1}} - y_{b_i}\right)$$

$$(47)$$

The total force coefficients in the x and y directions are of course given by summing the above expressions over the total number of elements of interest, NE, and the result is

$$C_x = \sum_{i=1}^{NE} C_{x_i}$$
$$C_y = \sum_{i=1}^{NE} C_{y_i}$$

$$(48)$$

Sensitivity derivatives of these force coefficients taken with respect to β_k are given as

$$\frac{dC_x}{d\beta_k} = \sum_{i=1}^{NE} \left\{ \frac{\partial C_{P_i}}{\partial \beta_k}\left(y_{b_{i+1}} - y_{b_i}\right) + C_{P_i}\left(\frac{\partial y_{b_{i+1}}}{\partial \beta_k} - \frac{\partial y_{b_i}}{\partial \beta_k}\right) \right\}$$
$$+ \sum_{i=1}^{NE} \left\{ \frac{\partial C_{f_i}}{\partial \beta_k}\left(x_{b_{i+1}} - x_{b_i}\right) + C_{f_i}\left(\frac{\partial x_{b_{i+1}}}{\partial \beta_k} - \frac{\partial x_{b_i}}{\partial \beta_k}\right) \right\}$$

$$(49)$$

$$\frac{dC_y}{d\beta_k} = \sum_{i=1}^{NE} \left\{ \frac{\partial C_{P_i}}{\partial \beta_k}\left(x_{b_i} - x_{b_{i+1}}\right) + C_{P_i}\left(\frac{\partial x_{b_i}}{\partial \beta_k} - \frac{\partial x_{b_{i+1}}}{\partial \beta_k}\right) \right\}$$
$$+ \sum_{i=1}^{NE} \left\{ \frac{\partial C_{f_i}}{\partial \beta_k}\left(y_{b_{i+1}} - y_{b_i}\right) + C_{f_i}\left(\frac{\partial y_{b_{i+1}}}{\partial \beta_k} - \frac{\partial y_{b_i}}{\partial \beta_k}\right) \right\}$$

Note in the above expressions that terms such as $\frac{\partial x_{b_i}}{\partial \beta_k}$, $\frac{\partial y_{b_i}}{\partial \beta_k}$, etc., are evaluated as being elements of the vector $\left\{\frac{\partial \bar{X}}{\partial \beta_k}\right\}$ of the previously discussed right–hand side of Eq. (16), (18), or (21) and $\frac{\partial C_{p_i}}{\partial \beta_k}$ and also $\frac{\partial C_{f_i}}{\partial \beta_k}$ are obtained from the vector $\left\{\frac{\partial \bar{Q}^*}{\partial \beta_k}\right\}$ by solution of these equations. (Note: Since C_{f_i} involves <u>gradients</u> of the velocity at the ith element of the boundary, then $\frac{\partial C_{f_i}}{\partial \beta_k}$ involves terms from both $\left\{\frac{\partial \bar{Q}^*}{\partial \beta_k}\right\}$ and $\left\{\frac{\partial \bar{X}}{\partial \beta_k}\right\}$, resulting in an expression not shown here which is algebraically complex.)

If the sensitivity derivatives of the lift (C_L) and drag (C_D) coefficients of a body (e.g., an airfoil) are desired, it is only necessary to convert to a new coordinate system with axes aligned

in the L and D directions, which are rotated at an angle of attack, α, with respect to the x and y axes. The lift and drag coefficients are then calculated as

$$C_L = C_y \cos \alpha - C_x \sin \alpha \tag{50}$$

$$C_D = C_y \sin \alpha + C_x \cos \alpha \tag{51}$$

The corresponding expressions for the sensitivity derivatives of the lift and drag coefficients are

$$\frac{dC_L}{d\beta_k} = \frac{dC_y}{d\beta_k} \cos \alpha - \frac{dC_x}{d\beta_k} \sin \alpha \tag{52}$$

$$\frac{dC_D}{d\beta_k} = \frac{dC_y}{d\beta_k} \sin \alpha + \frac{dC_x}{d\beta_k} \cos \alpha \tag{53}$$

Note Eqs. (64) and (65) are not valid if the angle of attack, α, is the design variable (i.e., if $\alpha = \beta_k$). In this special case, these expressions would simply have additional terms. (See Eq. (33).)

In addition, for airfoil calculations, the sensitivity derivatives of the pitching moment coefficient, C_M, could likely be of interest in a design problem. The moment coefficient, C_{M_i}, which is associated with the ith element (see Fig. (6)) on the solid wall boundary of interest, about the point (x_o, y_o), with the convention that a positive moment is clockwise, is given by

$$C_{M_i} = C_{x_i}(y_{c_i} - y_o) - C_{y_i}(x_{c_i} - x_o) \tag{54}$$

where the coordinate (x_{c_i}, y_{c_i}) is the <u>midpoint</u> of the ith element on the boundary. That is

$$x_{c_i} = \frac{1}{2}(x_{b_{i+1}} + x_{b_i}) \qquad y_{c_i} = \frac{1}{2}(y_{b_{i+1}} + y_{b_i}) \tag{55}$$

The total moment coefficient is of course the sum of all the elemental moment coefficients over the total number of elements on the boundary of interest, given by

$$C_M = \sum_{i=1}^{NE} C_{M_i} \tag{56}$$

The sensitivity derivative of the pitching moment coefficient with respect to the kth design variable is thus

$$\frac{dC_M}{d\beta_k} = \sum_{i=1}^{NE} \left\{ \frac{\partial C_{x_i}}{\partial \beta_k} (y_{c_i} - y_o) + C_{x_i} \frac{\partial y_{c_i}}{\partial \beta_k} \right\} - \sum_{i=1}^{NE} \left\{ \frac{\partial C_{y_i}}{\partial \beta_k} (x_{c_i} - x_o) + C_{y_i} \frac{\partial x_{c_i}}{\partial \beta_k} \right\} \tag{57}$$

where

$$\frac{\partial x_{c_i}}{\partial \beta_k} = \frac{1}{2} \left(\frac{\partial x_{b_{i+1}}}{\partial \beta_k} + \frac{\partial x_{b_i}}{\partial \beta_k} \right) \qquad \frac{\partial y_{c_i}}{\partial \beta_k} = \frac{1}{2} \left(\frac{\partial y_{b_{i+1}}}{\partial \beta_k} + \frac{\partial y_{b_i}}{\partial \beta_k} \right) \tag{58}$$

In the present study, an internal flow problem was considered where the sensitivity derivatives of the thrust, T, mass flow rate, $\dot{m}$, and specific thrust, F_s, of a nozzle are of interest, and the xpressions used in these calculations are developed next. The total thrust which is produced by a nozzle can be calculated from the previously defined force coefficient, C_x, summed over all of the interior solid walls, plus an additional term involving the integrated static pressure over the inflow boundary of the nozzle. That is

$$T = -C_x + \sum_{j=1}^{NEJ} C_{p_j}(y_{j+1} - y_j) \tag{59}$$

where in the above, a positive thrust acts in a direction opposite to the positive direction of the x axis, the y axis is assumed to be in or parallel to the plane of the inflow boundary, C_{p_j} is the static pressure coefficient of the jth element on the inflow boundary, y_j and y_{j+1} are the starting and ending coordinates, respectively, of the jth element on the inflow, where the direction of increasing the index, 'j', and the positive y direction are in this case defined to be always the same, and NEJ is the total number of elements on the inflow boundary. Nondimensionalization of T in Eq. (59) above is of course the same as defined previously for C_x. (Note: The expression above does not consider the aerodynamic forces, if any, due to flow over the exterior surfaces of the nozzle.) The sensitivity derivative of the thrust is

$$\frac{dT}{d\beta_k} = -\frac{dC_x}{d\beta_k} + \sum_{j=1}^{NEJ} \frac{\partial C_{p_j}}{\partial \beta_k}(y_{j+1} - y_j) + \sum_{j=1}^{NEJ} C_{p_j} \left(\frac{\partial y_{j+1}}{\partial \beta_k} - \frac{\partial y_j}{\partial \beta_k} \right) \tag{60}$$

29

The mass flow rate, ṁ, through the nozzle can be computed using the expression

$$\dot{m} = \sum_{j=1}^{NEJ} \rho_j \, u_j (y_{j+1} - y_j) \tag{61}$$

and the sensitivity derivatives become

$$\frac{d\dot{m}}{d\beta_k} = \sum_{j=1}^{NEJ} \rho_j u_j \left(\frac{\partial y_{j+1}}{\partial \beta_k} - \frac{\partial y_j}{\partial \beta_k} \right) + \sum_{j=1}^{NEJ} \rho_j \frac{\partial u_j}{\partial \beta_k} (y_{j+1} - y_j) + \sum_{j=1}^{NEJ} \frac{\partial \rho_j}{\partial \beta_k} u_j (y_{j+1} - y_j) \tag{62}$$

Often with nozzle calculations, the specific thrust, F_s, is a system response of interest, and is defined by

$$F_s = \frac{T}{\dot{m}} \tag{63}$$

and the sensitivity derivatives can be calculated using expressions previously defined

$$\frac{dF_s}{d\beta_k} = \frac{\dot{m} \frac{dT}{d\beta_k} - T \frac{d\dot{m}}{d\beta_k}}{\dot{m}^2} \tag{64}$$

3.0 Computational Results

3.1 Internal Flow — Double-Throat Nozzle Problem

3.1.1 Description of the Test Problem

The first test problem to be presented is that of an internal flow through a double-throat nozzle, where the flow is accelerated from a Mach number on the inflow boundary of about 0.10, to a Mach number which exceeds 2.80 at some places on the outflow. The Reynolds number, RE_L, is 100, based on a reference length, L, of one-half the height of the nozzle at the smaller of the two throats. Other researchers have conducted numerical studies on the flow through this nozzle geometry, with documentation provided in Refs. [5,45,46,47].

30

A computational grid is used with 171 points evenly spaced in the streamwise direction, and 38 points with grid stretching in the normal direction, to resolve viscous gradients in the vicinity of solid walls. Fig. (7) illustrates the grid and geometry. Boundary conditions are specified as follows:

1) On the inflow, entropy and stagnation enthalpy are held constant at the freestream values, the v component of velocity is zero, and the u component is extrapolated from the interior of the domain.

2) On the outflow boundary, all variables are extrapolated.

3) On the lower wall, velocity no-slip is enforced, and the wall static temperature is specified to be that of the stagnation temperature of the freestream.

4) On the upper boundary of the computational domain (i.e., along the centerline of the nozzle), flow symmetry boundary conditions are enforced.

The Mach contours for the steady-state laminar flow solution through the nozzle are shown in Fig. (8).

The geometry of the nozzle is defined parametrically using analytical expressions which are presented subsequently, where this material is also given in Ref. [47]. Because of symmetry, it is only necessary to parameterize either the lower or the upper solid wall surface. The upper wall is selected here. The wall is described using five polynomial arcs, as illustrated in Fig. (9). In all cases, continuity of slope is enforced at the transition point from one arc to the next. Continuity of curvature is also preserved at the transition point from arc II to arc III and from arc III to arc IV, but is discontinuous as the transition from arc I to arc II and from arc IV to arc V. Using Fig. (9), these five arcs are defined as follows

$$\textbf{ARC III} \quad (X_3 \leq X \leq X_4)$$

$$Y = H + \left(\frac{A}{2}\right) X^2 \left[\frac{X^2}{6} - \left(\frac{X_3 + X_4}{3}\right) X + X_3 X_4\right] \tag{65}$$

31

From Eq. (65), the following is deduced

$$Y(X_3) = H + \left(\frac{A}{6}\right)(X_3)^3\left(2X_4 - \frac{X_3}{2}\right)$$

$$Y_x(X_3) = \left(\frac{A}{2}\right)(X_3)^2\left(X_4 - \frac{X_3}{3}\right)$$

$$Y(X_4) = H + \left(\frac{A}{3}\right)(X_4)^3\left(X_3 - \frac{X_4}{4}\right)$$

$$Y_x(X_4) = \frac{A}{2}(X_4)^2\left(X_3 - \frac{X_4}{3}\right)$$

(66)

where in the above and henceforth the subscript x indicates differentiation with respect to X (i.e., $Y_x = \frac{dY}{dX}$).

$$\textbf{ARC II} \quad (X_2 \leq X \leq X_3)$$

$$Y = Y(X_3) + Y_x(X_3)(X - X_3)\left[1 - \left(\frac{1}{3}\right)\left(\frac{X - X_3}{X_2 - X_3}\right)^2\right] \quad (67)$$

From Eq. (67), the following is noted

$$Y(X_2) = Y(X_3) + \frac{2}{3}(X_2 - X_3)Y_x(X_3) \quad (68)$$

$$\textbf{ARC I} \quad (X_1 \leq X \leq X_2)$$

$$Y = Y(X_2) \quad (69)$$

$$\textbf{ARC IV} \quad (X_4 \leq X \leq X_5)$$

$$Y = Y(X_4) + (X - X_4)\left[Y_x(X_4) + B(Z_1)^2 + C(Z_1)^3\right] \quad (70)$$

where

$$Z_1 = (X - X_4)/(X_5 - X_4)$$

$$B = 4D - 3Y_x(X_4)$$

$$C = -3D + 2Y_x(X_4) \quad (71)$$

$$D = [Y(X_5) - Y(X_4)]/(X_5 - X_4)$$

Note that X_5 is the location of the second throat, and $Y(X_5)$ represents the half-height of this second throat.

32

$$\textbf{ARC V} \quad (X_5 \leq X \leq X_6)$$

$$Y = Y(X_5) + [Y(X_6) - Y(X_5)](Z_2)^3(2 - Z_2) \tag{72}$$

where

$$Z_2 = (X - X_5)/(X_6 - X_5) \tag{73}$$

As a consequence of the above relationships, there are ten geometric shape parameters which can be identified from these expressions, which in the present work will also define the elements of the vector $\vec{\beta}$, known here as the <u>design</u> variables. These parameters are given below, including their numerical values for the "baseline" test geometry (i.e., the "initial design" of the nozzle).

$$\vec{\beta} = [\beta_1, \beta_2, \beta_3, \beta_4, \beta_5, \beta_6, \beta_7, \beta_8, \beta_9, \beta_{10}]^{\mathrm{T}} \tag{74}$$

where

$$\beta_1 = H = +1.0$$

$$\beta_2 = X_3 = -4.0$$

$$\beta_3 = X_4 = +2.3$$

$$\beta_4 = A = -0.03$$

$$\beta_5 = X_2 = -10.0$$

$$\beta_6 = X_1 = -12.0 \tag{75}$$

$$\beta_7 = X_5 = +7.0$$

$$\beta_8 = Y(X_5) = +1.6$$

$$\beta_9 = X_6 = +14.0$$

$$\beta_{10} = Y(X_6) = +5.85$$

3.1.2 Calculation and Validation of Sensitivity Derivatives

A study is conducted to validate the methodology which has been described herein for computing aerodynamic sensitivity derivatives, and to evaluate the efficiency of the procedures. In this study, geometric shape sensitivity derivatives are calculated using direct solution of Eq. (18) (together with some of the ancillary sensitivity equations presented in a previous subsection), and are also computed using the method of "brute force" finite differences. In applying the method of finite differences, in order to insure great accuracy, central differences are used (requiring two CFD analyses per design variable) with an extremely small perturbation of each design variable, and the repeated CFD analyses are converged to machine zero. Sensitivity derivatives taken with respect to the ten previously described geometric shape design variables (Eqs. (65) through (75)) are computed using these two methods, and are compared in Tables I, II, III, and IV. In Tables I and II, the sensitivity derivatives of C_x and C_y, respectively, for the lower wall of the nozzle are presented (C_x and C_y are aerodynamic force coefficients in the x and y directions, respectively, resulting from the integration of pressure and skin friction along the wall, and have been detailed previously.) In Tables III and IV, the sensitivity derivatives of the thrust, T, and the mass flow rate, $\dot{m}$, of the nozzle are given.

Design Variable	X-Direction Force Coefficient Sensitivity $\dfrac{dC_x}{d\beta_k}$	
	Direct Differentiation	Finite Difference
β_1	-4.925 E+01	-4.925 E+01
β_2	-4.614 E+02	-4.614 E+02
β_3	+2.284 E+02	+2.284 E+02
β_4	-2.665 E+04	-2.665E+04
β_5	-8.327 E+01	-8.327 E+01
β_6	-1.365 E-02	-1.365 E-02
β_7	+1.415 E+00	+1.415 E+00
β_8	+6.235 E+00	+6.235 E+00
β_9	-2.107 E+00	-2.107 E+00
β_{10}	+3.886 E-01	+3.886 E-01

Table I – Comparison of the X-direction Force Coefficient, C_x, Sensitivity Derivatives, Lower Wall, Double-Throat Nozzle, Laminar Flow

Design Variable	Y-Direction Force Coefficient Sensitivity $\dfrac{dC_y}{d\beta_k}$	
	Direct Differentiation	Finite Difference
β_1	-3.024 E+02	-3.024 E+02
β_2	+1.741 E+01	+1.741 E+01
β_3	-2.625 E+01	-2.625 E+01
β_4	+1.664 E+03	+1.664 E+03
β_5	+4.365 E-01	+4.365 E-01
β_6	+1.428 E+02	+1.428 E+02
β_7	-5.879 E+00	-5.879 E+00
β_8	+2.331 E+02	+2.331 E+02
β_9	-2.081 E+01	-2.081 E+01
β_{10}	+1.158 E+01	+1.158 E+01

Table II – Comparison of the Y-direction Force Coefficient, C_y, Sensitivity Derivatives, Lower Wall, Double-Throat Nozzle, Laminar Flow

Design Variable	Thrust Sensitivity $\dfrac{dT}{d\beta_k}$	
	Direct Differentiation	Finite Difference
β_1	+1.841 E+02	+1.841 E+02
β_2	-4.869 E+00	-4.869 E+00
β_3	+2.783 E+00	+2.782 E+00
β_4	-3.254 E+02	-3.254 E+02
β_5	-7.304 E-01	-7.303 E-01
β_6	-2.879 E-02	-2.878 E-02
β_7	-1.415 E+00	-1.415 E+00
β_8	-6.235 E+00	-6.235 E+00
β_9	+2.106 E+00	+2.106 E+00
β_{10}	-3.886 E-01	-3.886 E-01

Table III – Comparison of the Thrust Sensitivity Derivatives, Double-Throat Nozzle, Laminar Flow

Design Variable	Mass Flow Rate Sensitivity $\dfrac{d\dot{m}}{dJ_k}$	
	Direct Differentiation	Finite Difference
J_1	+5.701 E+00	+5.701 E+00
J_2	-1.639 E-02	-1.639 E-02
J_3	+2.819 E-02	+2.819 E-02
J_4	-2.168 E+00	-2.168 E+00
J_5	-1.933 E-05	-1.895 E-05
J_6	-1.172 E-04	-1.171 E-04
J_7	-1.096 E-09	+0.000 E+00
J_8	-4.158 E-09	-5.684 E-09
J_9	+1.131 E-04	+1.134 E-04
J_{10}	-8.740 E-13	+0.000 E+00

Table IV – Comparison of the Mass Flow Rate Sensitivity
Derivatives, Double-Throat Nozzle, Laminar Flow

As expected, the agreement in the results above obtained using the two methods is excellent. The results only disagree for some of the mass flow rate sensitivities when these sensitivity derivatives are negligibly small. Table V is a comparison of the total CPU times which where required to obtain one complete set of sensitivity derivatives. Clearly the direct differentiation approach is more efficient in this problem. However, due to the extreme care which was taken in insuring accuracy when using the finite difference approach, the CPU time reported here for this method should be taken as an upper bound "worst case".

CPU Time	Direct Differentiation	Finite Difference
	- 65 seconds	- 1800 seconds

Table V – Comparison of CPU times, Double-Throat
Nozzle, Laminar Flow

The direct differentiation approach of Eq. (18) has now been shown to efficiently and accurately yield aerodynamic sensitivity derivatives for 2D viscous internal flows which are laminar. This is the expected result, since the exact derivatives are found of the discrete algebraic

equations which model the fluid flow. Unfortunately, however, a majority of the practical flow problems of interest in aerodynamic design are turbulent flows. If turbulence modeling is to be included in the flow calculations, then in principle, the equations which are used in the turbulence model which is selected should be consistently differentiated, and the results fully incorporated into the Jacobian matrices, $\left[\frac{\partial R}{\partial Q}\right]$ and $\left[\frac{\partial R}{\partial X}\right]$, of the fundamental sensitivity analysis / approximate analysis equations (i.e., Eqs. (16) through (21)). In practice, of course, for typical turbulence models, this represents a very difficult task, even impossible in the case of turbulence models which are not continuously differentiable (e.g., the popular Baldwin-Lomax model). For this reason, in typical CFD codes, consistent linearization of the turbulence modeling is neglected in the construction of the implicit terms of the matrix, $\left[\frac{\partial R}{\partial Q}\right]$, of Eq. (12) for the integration of the equations in time. Of course, the explicit spatial variation of the turbulence modeling terms which is found in the residual vector on the right-hand side of Eq. (12) is also used on the left-hand side in the terms of the Jacobian matrix, $\left[\frac{\partial R}{\partial Q}\right]$.

As a potentially useful simplifying approximation in the calculation of sensitivity derivatives for turbulent flows, an approach analogous to that described above for implicit time integration schemes is proposed. That is, differentiation of the turbulence modeling is neglected in the construction of the terms of the Jacobian matrices, $\left[\frac{\partial R}{\partial Q}\right]$, and $\left[\frac{\partial R}{\partial X}\right]$, of Eqs. (16) through (21). The explicit spatial variation of the steady-state values of the turbulence modeling terms is used, however, in both of these Jacobian matrices. This approximation is equivalent to a "locally constant" assumption applied to these terms.

In order to judge the error in the sensitivity derivatives which might be expected in using this approximation, a preliminary investigation is conducted using the present double-throat nozzle problem, and the Baldwin-Lomax turbulence model [21]. Strictly speaking, this turbulence model is not applicable to the present low Reynolds number problem, but this does not conflict with the goals of this preliminary investigation into the effect of turbulence models on the accuracy of the sensitivity derivatives.

37

To begin the study, a converged steady-state numerical solution using the Baldwin-Lomax turbulence model is obtained for the previously described problem of laminar flow through the double-throat nozzle. Sensitivity derivatives are obtained for the turbulent case with respect to the same ten geometric shape design variables as for the laminar problem, again using the direct differentiation approach of Eq. (18), and also using the method of "brute force" finite differences. In using Eq. (18), the approximate treatment of the turbulence modeling terms is employed, as previously proposed. Tables VI and VII are a presentation and comparison of the computational results obtained using these two methods, where the sensitivity derivatives of the thrust and mass flow rate, respectively, are shown.

Design Variable	Thrust Sensitivity $\dfrac{dT}{d\beta_k}$	
	Direct Differentiation	Finite Difference
β_1	+1.823 E+02	+1.821 E+02
β_2	-4.682 E+00	-4.788 E+00
β_3	+1.996 E+00	+2.645 E+00
β_4	-2.961 E+02	-3.140 E+02
β_5	-7.296 E-01	-7.296 E-01
β_6	-5.707 E-02	-2.470 E-02
β_7	-1.402 E+00	-1.475 E+00
β_8	-3.074 E-00	-3.624 E-00
β_9	+1.815 E+00	+1.889 E+00
β_{10}	-2.627 E-01	-2.705 E-01

Table VI – Comparison of the Thrust Sensitivity Derivatives, Double-Throat Nozzle, Turbulent Flow

Design Variable	Mass Flow Rate Sensitivity $\dfrac{d\dot{m}}{d\beta_k}$	
	Direct Differentiation	Finite Difference
β_1	+5.703 E+00	+5.697 E+00
β_2	-1.699 E-02	-1.641 E-02
β_3	+2.894 E-02	+2.841 E-02
β_4	-2.238 E+00	-2.187 E+00
β_5	-2.317 E-05	-2.463 E-05
β_6	-6.753 E-04	-1.516 E-04
β_7	-5.658 E-10	+0.000 E+00
β_8	-1.949 E-09	-4.263 E-09
β_9	+2.816 E-04	+1.045 E-04
β_{10}	-2.084 E-13	-1.421 E-09

Table VII – Comparison of the Mass Flow Rate Sensitivity
Derivatives, Double-Throat Nozzle, Turbulent Flow

Note that in generating the "brute force" sensitivity derivatives shown in Table VI and VII, the same extreme care was taken to insure great accuracy of the terms that was taken previously for the laminar results. Therefore, the "brute force" values shown for the turbulent case are considered to be more accurate than the values obtained using the method of direct differentiation (because of the approximate treatment of the turbulence modeling terms which was used in the latter approach). In general, however, the agreement between the two methods is reasonably good, hopefully good enough for future use in a design optimization strategy.

3.1.3 Optimization Problem — Double-Throat Nozzle

Having verified the accuracy and efficiency of the methodology for computing sensitivity derivatives, a short study is conducted to demonstrate the application of the sensitivity derivatives in a model optimization example problem, using the double-throat nozzle described above. A generalized procedure is proposed for aerodynamic design optimization, where the principal computational tasks are sub-divided into distinct modules, or major subroutines, all controlled by a central, external, general purpose design optimization computer program. The well-known

design optimization program selected for use in the present study is called ADS (Automated Design Synthesis), which is documented in Ref. [48], although others are available.

The principal computational tasks to be performed dynamically in the automated aerodynamic design strategy are accomplished using a standard CFD code (in order to re-evaluate the aerodynamic performance variables), a sensitivity analysis program, based on the CFD analysis code (for computing the sensitivity derivatives required by the optimization program), a grid regeneration program (for shape optimization, as the shape of the domain changes) and grid sensitivity capability (necessary in computing shape sensitivity derivatives). In addition, an optional approximate analysis capability (based on Eqs. (19) or (21), for geometric shape changes) can be included as a subset of the sensitivity analysis module, in order to provide significantly more efficient re-evaluation of the aerodynamic performance variables, when the changes in the design variables are small (i.e., less than some specified tolerance). The validity, accuracy, and efficiency of the approximate analysis methodology is documented in Refs. [3,5,6,7]. The proposed aerodynamic design optimization strategy is illustrated in Fig. (10).

Starting with the initial nozzle shape and steady-state solution, the proposed aerodynamic shape optimization method of Fig. (10) is applied to the nozzle problem, as follows:

1) The force coefficient in the x direction, C_x, (henceforth known as the objective function), is to be minimized in the design, subject to the explicit constraints on the design variables, given subsequently. C_x represents the internal aerodynamic drag on the lower wall of the nozzle.

2) The design variables are the ten elements of $\vec{\beta}$, defined in Eq. (75), and an upper and lower bound is placed on each, where the total maximum allowable change in each during the design, either an increase or decrease, is specified a priori to be no greater than 15% of the initial value of each variable.

3) Sensitivity derivatives with respect to the design variables of the objective function are obtained using the method of direct differentiation (Eq. (18)) and the ancillary sensitivity equations given previously. Sensitivity derivatives of the explicit constraints (i.e., the

upper and lower bounds) on the design variables are not needed, as they do not change during optimization.

4) Mesh regeneration and grid sensitivity derivatives are provided by the grid generation computer program which produced the initial mesh, and grid sensitivity is obtained using this program and the "brute force" approach (i.e., Eq. (37)).

Following application of the automated design optimization strategy, the results are summarized in Tables VIII and IX.

Performance Variable	Initial Design	Final Design	Percent Change
Force Coefficient, C_x (Objective Function)	+754.4	+313.9	-58.39
Thrust, T	+190.4	+205.4	+7.88
Mass Flow Rate, $\dot{m}$	+5.463	+6.284	+15.0
Specific Thrust, F_s	+34.85	+32.69	-6.20

Table VIII – Comparison of the Aerodynamic Performance of the Initial and Final Designs, Nozzle Problem

Design Variable	Initial Design	Final Design	Percent Change
β_1	+1.0	+1.150	+15.00
β_2	-4.0	-3.400	+15.00
β_3	+2.3	+2.017	-12.30
β_4	-0.03	-0.0255	+15.00
β_5	-10.0	-8.500	+15.00
β_6	-12.0	12.000	0.0
β_7	+7.0	+7.000	0.0
β_8	+1.6	+1.599	-0.0625
β_9	+14.0	+14.000	0.0
β_{10}	+5.85	5.850	0.0

Table IX – Comparison of the Initial and Final Design Variables, Nozzle Problem

41

Clearly a significant reduction in the aerodynamic drag on the internal walls of the nozzle (as defined in the present problem statement) was achieved, as demonstrated by the desired reduction in the objective function in the new design. Figs. (11a) and (11b) represent a comparison of the geometric shapes of the initial and final nozzle designs, respectively. (Fig. (11a) is a repeat of Fig. (7).) In reducing the aerodynamic drag on the internal walls of the nozzle, the shape of the final design clearly displays a predictable pattern of "smoothing out the bumps" in the contours of the walls. Had the explicit bounds on the design variables been removed, this effect would surely have been even greater. The results shown here were obtained following only three evaluations of the objective function (following the initial evaluation). The option of approximate analysis was not used in the present test problem.

In the present model design problem, aerodynamic drag reduction is considered, as it is of general interest in many aerodynamic design problems. In the design of nozzles, however, clearly the thrust, mass flow rate, and specific thrust, F_s, ($F_s = T/\dot{m}$) are variables of special interest to the designer. For this reason, the values of these variables for the initial and final designs have been included in Table VIII. A more realistic shape optimization problem for nozzles might typically select the maximization of F_s as the objective function, perhaps with the side constraint that the thrust of the final design be no less than that of the initial design. Reformulation of the present test problem in this manner is straightforward, in principle, since the sensitivity derivatives of these terms are available (i.e., thrust and mass flow rate sensitivities have been presented herein, from which specific thrust sensitivities are obtained using Eq. (64).

3.2 External Flow — NACA 4-Digit Airfoil Problem

3.2.1 Description of the Test Problem

The external flow problem which is studied in the present work is that of an isolated airfoil. The initial airfoil which is selected is the NACA 2412, the profile of which is defined by Eqs. (41) and (42), with maximum thickness, $T = 0.12$, maximum camber, $C = 0.02$, and location of maximum camber, $L = 0.40$. The computations are performed on a "C" mesh using 128 points

in the "around the airfoil" direction, (with 68 of these on the surface of the airfoil) and 32 points in the normal to the airfoil direction, with grid stretching near the airfoil surface. The far-field boundary is placed twenty chords from the airfoil. The grid is generated using the algebraic mesh generation program of Ref. [42]. The grid used in the present test case is clearly inadequate for use in resolving the full physics of viscous flow over an airfoil. Therefore, it should be understood that the objective of the work for which results are to be presented is $\underline{not}$ at this point to produce highly accurate calculations of the flow field. The objective rather is to successfully implement, demonstrate, and validate the ideas on a computationally inexpensive model problem.

A converged conventional numerical solution is obtained for the initial geometry and grid for laminar flow, for a freestream Mach number, $M_\infty = 0.70$, Reynolds number, $RE_L = 5000.$, and angle of attack $\alpha = 0.0°$. Boundary conditions on the airfoil surface, across the "wake-cut", and at the far-field boundaries have been discussed previously. When the "lift corrected" far-field boundary conditions are $\underline{not}$ used, the lift (C_L), drag (C_D), and moment (C_M) coefficients for the calculation were $C_L = 0.1232$, $C_D = 0.06824$, and $C_M = -0.05328$. When the lift correction of Ref. [40] $\underline{is}$ applied at the far-field boundaries, these coefficients become $C_L = 0.1252$, $C_D = 0.06821$, and $C_M = -0.05325$. Therefore, the numerical effect of the far-field lift correction is not strong in this example problem, which is attributed to the rather large extent of the far-field boundary from the airfoil (twenty chords) which was used. This effect will become more significant, however, as the far-field boundary is brought closer to the airfoil surface [40], i.e., the lift-corrected boundary conditions become more necessary. Of course, the freedom to move the far-field boundary closer to the airfoil surface allows more effective use of the grid points which are available, in order to more accurately resolve the flow physics.

3.2.2 Calculation and Validation of Sensitivity Derivatives

A study is conducted to validate the methodology which has been described herein for computing aerodynamic sensitivity derivatives for airfoils, and to evaluate the efficiency of the procedures. Unless otherwise stated, sensitivity derivatives are computed using the steady-state solution $\underline{without}$ the point-vortex lift-corrected far-field boundary conditions. In particular,

geometric shape sensitivity derivatives are calculated by solution of Eq. (18) using the hybrid direct solver / iterative strategy proposed in Eq. (30) (and also using some of the ancillary sensitivity equations presented previously). For comparison purposes, the sensitivity derivatives are also computed using the "brute force" method of finite differences. In applying this approach, to insure good accuracy, central finite difference approximations are used with a forward and backward perturbation of each design variable of 0.01%, and the repeated CFD analyses are converged to machine zero.

The sensitivity derivatives of the lift, drag, and moment coefficients are computed with respect to the three geometric shape parameters, T, C, and L of Eqs. (41) and (42) using the initial airfoil, grid, and flow conditions which have been described immediately above. In solving Eq. (18), the required grid sensitivity terms (i.e., $\left\{\frac{\partial X}{\partial \beta_k}\right\}$) were provided using the previously described "elastic membrane" representation of the computational domain, and the prescribed displacement approach, together with Eqs. (39) through (45). In addition, as a consistency requirement, this grid methodology is also used in generating the necessary "perturbed" grids which are required in computing aerodynamic sensitivity derivatives by the "brute force" approach.

When solving Eq. (18) using the hybrid direct solver / iterative method of Eq. (30), it is necessary to establish some type of criterion by which the iterative solution of the linear system for each design variable is judged to be "converged," and is terminated. To study this, the sensitivity derivatives are calculated with Eq. (30) using progressively stricter convergence criteria, starting with a calculation where no iterations are used (i.e., the "periodic" terms outside of the central bandwidth are simply neglected) and ending with a calculation where the average global error is reduced four orders-of-magnitude. A summary of these calculations, including the results of the finite difference approach, is presented in Tables X, XI, and XII, one table for each of the three geometric shape design variables, T, C, and L, respectively.

As expected, as the reduction in the error by the iterative process defined by Eq. (30) is increased, the agreement between the sensitivity derivatives calculated using the method of direct

differentiation (Eq. (18)) and the same terms calculated using the method of finite differences is excellent. In addition, the validity of the "elastic membrane" methodology for computing grid sensitivities is confirmed. Furthermore, in the present problem, it is demonstrated that 1) approximately a three orders-of-magnitude reduction in the error is more than satisfactory for engineering purposes in applying Eq. (30), but 2) complete neglect of the implicit periodic boundary condition terms is completely unacceptable in using Eq. (18) to predict the sensitivity derivatives (Note: In contrast, these terms typically <u>are</u> neglected in the integration of the equations in time, using Eq. (12)).

Method of Solution	Lift Sensitivity $\frac{\partial C_L}{\partial \beta_1} = \frac{\partial C_L}{\partial T}$	Drag Sensitivity $\frac{\partial C_D}{\partial \beta_1} = \frac{\partial C_D}{\partial T}$	Moment Sensitivity $\frac{\partial C_M}{\partial \beta_1} = \frac{\partial C_M}{\partial T}$	No. of Iterations Using Eq. (30)
Eq. (30), Without Iterations	-9.334 E-01	+4.723 E-01	+9.815 E-02	1
Eq. (30), 1 OM	-2.859 E+00	+4.267 E-01	+4.755 E-01	13
Eq. (30), 2 OM	-3.117 E+00	+3.972 E-01	+5.278 E-01	64
Eq. (30), 3 OM	-3.126 E+00	+3.939 E-01	+5.307 E-01	219
Eq. (30), 4 OM	-3.126 E+00	+3.938 E-01	+5.307 E-01	300
Finite Difference	-3.126 E+00	+3.938 E-01	+5.307 E-01	N/A

*OM Refers to the number of Orders-of-Magnitude reduction in the average global error.

Table X – Comparison of Lift and Drag Sensitivity Derivatives
With Respect To Maximum Thickness, β_1=T, NACA 2412 Airfoil

Method of Solution	Lift Sensitivity $\frac{\partial C_L}{\partial \beta_2} = \frac{\partial C_L}{\partial C}$	Drag Sensitivity $\frac{\partial C_D}{\partial \beta_2} = \frac{\partial C_D}{\partial C}$	Moment Sensitivity $\frac{\partial C_M}{\partial \beta_2} = \frac{\partial C_M}{\partial C}$	No. of Iterations Using Eq. (30)
Eq. (30), Without Iterations	+5.206 E+00	+3.429 E-01	-2.520 E+00	1
Eq. (30), 1 OM	+4.175 E+00	+3.780 E-01	-2.261 E+00	14
Eq. (30), 2 OM	+3.988 E+00	+3.663 E-01	-2.225 E+00	39
Eq. (30), 3 OM	+3.968 E+00	+3.603 E-01	-2.220 E+00	188
Eq. (30), 4 OM	+3.968 E+00	+3.603 E-01	-2.220 E+00	276
Finite Difference	+3.968 E+00	+3.603 E-01	-2.220 E+00	N/A

*OM Refers to the number of Orders-of-Magnitude reduction in the average global error.

Table XI – Comparison of Lift and Drag Sensitivity Derivatives With Respect To Maximum Camber, β_2=C, NACA 2412 Airfoil

Method of Solution	Lift Sensitivity $\frac{\partial C_L}{\partial \beta_3} = \frac{\partial C_L}{\partial L}$	Drag Sensitivity $\frac{\partial C_D}{\partial \beta_3} = \frac{\partial C_D}{\partial L}$	Moment Sensitivity $\frac{\partial C_M}{\partial \beta_3} = \frac{\partial C_M}{\partial L}$	No. of Iterations Using Eq. (30)
Eq. (30), Without Iterations	-4.293 E-02	-3.899 E-03	-3.865 E-02	1
Eq. (30), 1 OM	-1.466 E-02	-3.422 E-03	-4.456 E-02	5
Eq. (30), 2 OM	-1.869 E-02	-3.334 E-03	-4.386 E-02	24
Eq. (30), 3 OM	-1.819 E-02	-3.304 E-03	-4.396 E-02	49
Eq. (30), 4 OM	-1.816 E-02	-3.290 E-03	-4.398 E-02	195
Finite Difference	-1.815 E-02	-3.290 E-03	-4.398 E-02	N/A

*OM Refers to the number of Orders-of-Magnitude reduction in the average global error.

Table XII – Comparison of Lift and Drag Sensitivity Derivatives With Respect To Location of Maximum Camber, β_3=L, NACA 2412 Airfoil

Table XIII is a comparison of the relative computational cost of obtaining the sensitivity derivatives using the procedures for which results have been given in the three preceding tables. In the present problem, clearly the finite difference method is less efficient than the use of Eq. (30), even when the required error reductions using Eq. (30) are specified to be large. However, because of the great care which was taken in applying the finite difference method to insure very accurate results (for validation purposes), the CPU times reported for this finite difference method should be taken to represent a "worst case" scenario.

Method of Solution	CPU Time, Total (seconds)
Eq. (30), Without Iterations	27
Eq. (30) 1 OM	33
Eq. (30) 2 OM	54
Eq. (30) 3 OM	124
Eq. (30) 4 OM	191
Finite Difference	840

*OM Refers to the number of Orders-of-Magnitude reduction in the average global error.

Table XIII – Comparison of CPU Times – Airfoil Problem

As mentioned earlier, in applying the hybrid direct solver / iterative strategy of Eq. (30) in the solution of Eq. (18), for the results presented above, it was necessary to use under-relaxation to force the iterations to converge. A single under-relaxation parameter, $\omega = 0.75$ was used. The required use of this parameter, in addition to the relatively large numbers of iterations (and hence the proportionally large amounts of CPU time) required in reducing the error to an acceptable level is worrisome, and was neither the expected nor the desired result. As stated earlier, these difficulties were not encountered in the related work of Ref. [33,39]. Additional work is needed to correct these difficulties, and to improve the efficiency of the algorithms for solving the equations of sensitivity analysis. Recent studies have cast these large

systems of linear equations in "delta" or "incremental" form [49,50], where it is seem that these difficulties with matrix ill-conditioning are overcome. This incremental formulation allows for the accurate efficient iterative solution of these equations using the identical <u>approximate</u> left-hand side coefficient matrix operator and algorithms which are commonly using in the numerical "time integration" of the non-linear flow equations to steady-state [26,27,34,35,36,37,38].

For airfoil design problems, if the sensitivity derivatives of only two or three performance variables (i.e., C_L, C_D, and maybe C_M) are needed, but the number of design variables is significantly larger than two or three, then the issue of a slow convergence rates during multiple iterative solutions of Eq. (30) can be addressed to a large extent by switching from the present method to the adjoint-variable method for computing the sensitivity derivatives [2,4]. The computational work of the adjoint-variable approach is completely independent of the number of design variables, and requires the solution (either directly or iteratively) of a single large system of linear equations (having coefficient matrix, $-\left[\frac{\partial R}{\partial Q}\right]^T$) for each aerodynamic performance variable for which the sensitivity derivatives are required, which as stated is typically only two or three variables, for airfoils. Clearly this is potentially a very large savings if the convergence rate of Eq. (30) is slow and the number of design variables is large.

The sensitivity derivatives of the steady-state solution <u>with</u> the lift-corrected far-field boundary conditions [40] was considered next, using the methodology proposed in Eqs. (31) through (33). The <u>modified</u> hybrid direct solver/conventional iterative solver strategy of Eqs. (35) (including Eq. (36)) was applied in the solution for the sensitivity derivatives. The results are summarized in Table XIV, where it is seen that the agreement in the calculations is very good in comparing the results obtained using Eqs. (35) and (36) (following a four orders-of-magnitude reduction in the average global error) with the results obtained using the method of "brute force" finite differences. Of additional interest is to compare the results of Table XIV with the corresponding results presented in Tables X, XI, and XII (i.e., the comparison is of the sensitivity derivatives of the solution with the lift-corrected boundary conditions with the sensitivity derivatives of the solution without this correction).

48

Solution Method	Design Variable	$\dfrac{dC_L}{dT.C.L}$	$\dfrac{dC_D}{dT.C.L}$	$\dfrac{dC_M}{dT.C.L}$
Eqs (35) and (36), 4 OM*	T	-3.211 E+00	+3.959 E-01	+5.337 E-01
	C	+4.015 E+00	+3.578 E-01	-2.216 E+00
	L	-1.751 E-02	-3.327 E-03	-4.410 E-02
"Brute Force," Finite Difference Method.	T	-3.211 E+00	+3.959 E-01	+5.337 E-01
	C	+4.015 E+00	+3.578 E-01	-2.217 E+00
	L	-1.752 E-02	-3.326 E-03	-4.410 E-02

*OM Refers to the number of Orders-of-Magnitude reduction in the average global error.

Table XIV – Comparison of the Sensitivity Derivatives With The Lift-Corrected Far-Field Boundary Conditions – Airfoil Problem

3.2.3 Optimization Problem — NACA 4-digit Airfoil

Having successfully validated the accuracy and efficiency of the proposed strategies for computing grid regeneration, grid sensitivity derivatives, and finally, aerodynamic sensitivity derivatives for isolated airfoils on "C" and "O" meshes, the application of these methods is demonstrated here in a model airfoil design optimization problem. The optimization strategy described previously for the nozzle test problem (and illustrated in Fig. (10)) is applied, using the NACA 2412 airfoil, grid, and steady-state solution described above as the initial design. The optimization problem is formulated as follows:

1) The lift coefficient, C_L, is to be maximized in response to geometric shape variations, subject to the design constraints defined subsequently.

2) The drag coefficient, C_D, is to be no greater than the value of the initial design.

3) The design variables (i.e., the elements of β) are the three parameters of the NACA 4-digit airfoil, i.e., T, C, and L, defined previously. The "linearized" NACA 4-digit

airfoil of Eqs. (43) and (44) defines the range of allowable airfoil shapes in terms of these three parameters. (As stated previously, this linearized equation only approaches the true NACA 4-digit parameterization of Eqs. (41) and (42) for small changes in the parameters, but the current parameterization is not limited to small changes). In addition, upper and lower bounds are defined a priori, for each of the design variables, as follows:

$$0.08 \leq T \leq 0.16$$

$$0.00 \leq C \leq 0.05$$

$$0.20 \leq L \leq 0.60$$

4) Sensitivity derivatives of the objective function, C_L, and the constraint, C_D, with respect to the design variables are obtain by solution of Eq. (18), using the hybrid direct solver / iterative strategy of Eq. (30). The global average error reduction in the solution of Eq. (18) is specified to be three orders-of-magnitude for each design variable. Sensitivity derivatives of the explicit constraints on the design variables (i.e., the upper and lower bounds) are not needed.

5) Mesh regeneration and grid sensitivity derivatives are provided dynamically during the automated optimization process using the finite element method and the "elastic membrane" prescribed displacement model of the computational grid, presented previously.

One important benefit and use of sensitivity analysis is the ability to study the sensitivity derivatives of the initial design before the design process begins, in order to identify which design variables are important (i.e., very sensitive) to the problem, and which are not. By this, often it can be safely judged that some of the design variables are unneeded, and can be eliminated from the problem.

As an example of this, examination of the sensitivity derivatives in Tables X, XI, and XII (or Table XIV) reveals that the lift and drag sensitivities are about two orders-of-magnitude smaller for the third design variable, L, compared to the sensitivity derivatives for the remaining two.

This means that the third design variable is not important to the current design problem, and for increased efficiency in the design, can be eliminated. To verify this, the design optimization methodology was implemented twice, once including the design variable, L, and once neglecting it completely (i.e., fixing it to be the value of the initial design). As expected, there was no significant difference following optimization in the final improved designs, either in aerodynamic performance, or in the final values of the remaining two design variables, when the third design variable was discarded from the problem. The results of the airfoil optimization shown subsequently in Tables XV and XVI are therefore for the case where the third design variable, L, has been dropped from the design problem.

Performance Variable	Initial Design	Improved Design	Percent Change
C_L, Lift Coefficeint (objective function)	0.1232	0.3658	+196.9
C_D, Drag Coefficient (a constraint)	0.06824	0.06791	-0.48
Lift/Drag Ratio	1.805	5.387	+198.4

Table XV – Comparison of the Aerodynamic Performance
of the Initial and Final Designs, Airfoil Problem

Design Variable	Initial Design	Improved Design	Percent Change
β_1=T	0.1200	0.0800	-33.33
β_2=C	0.0200	0.0455	+127.5
β_3=L	0.4000	0.4000	0.0

Table XVI – Comparison of the Initial and Final Designs Variables, Airfoil Problem

Clearly an airfoil shape having significantly improved aerodynamic performance for the given conditions has resulted from the automated design methodology, in the present test case, as demonstrated by the increased lift coefficient and lift / drag ratio of the new design. Figs. (12a)

and (12b) represent a comparison between the geometric shapes of the initial and final airfoil designs, respectively. The results shown here were obtained following only two evaluations of the objective function (following the initial evaluation). The option of approximate analysis was not used in the present test problem.

4.0 Summary and Conclusions

A gradient based design optimization strategy has been developed in detail for use in practical aerodynamic design problems, using the 2D thin-layer Navier-Stokes equations. The strategy is general in nature, and is based on the classic idea of constructing different modules for performing the major tasks such as function evaluation, function approximation and sensitivity analysis, mesh regeneration and grid sensitivity analysis, all driven and controlled by a general purpose design optimization program. The methodology has been successfully demonstrated on both an internal and an external flow problem, where in each case, a significant improvement in aerodynamic performance was achieved.

In developing the methods which have been presented herein, the major effort has been focused on techniques for efficiently and accurately calculating the necessary sensitivity derivatives for use by the optimization program. In particular, much effort was spent in successfully developing and implementing a consistent treatment of the boundary conditions in the calculation of the aerodynamic sensitivity derivatives for the classic problem of external flow over an isolated lifting airfoil on "C" or "O" meshes. As a minor extension of the methodology for computing the sensitivity derivatives, an efficient strategy for approximate analysis is available, a capability which is potentially very useful in a design environment.

One of the most difficult design variables to consider is that of geometric shape, which has been the emphasis of the present work. With geometric shape, the issue of grid sensitivity analysis and grid regeneration must be considered in the development of an automated gradient based optimization scheme. In the present work, an efficient method for handling this difficulty based on well-known ideas from the discipline of structural shape design optimization has been

successfully applied to the aerodynamic design problem. The technique employs the finite element method, and an elastic membrane representation of the computational domain.

The investigation which has been presented herein is still in its initial stages, and there is an unlimited amount left to be done. For example, for the viscous airfoil problem which was presented herein, the grid was of insufficient size to truly resolve the full physics of a viscous flow. Future work will focus on implementation of the methods demonstrated here to full scale grids. A more complete parameterization of the airfoil boundary with more design variables is to be used, in order to increase the range of the design space. Design with turbulence modeling will be attempted. Finally, development of more efficient strategies (with respect to computational work and computer storage) for computing the sensitivity derivatives is underway.

5.0 Acknowledgments

6.0 References

1. Taylor, A.C. III, Hou, G.W., and Korivi, V.M., "Sensitivity Analysis, Approximate Analysis, and Design Optimization for Internal and External Viscous Flows," AIAA Paper 91-3083.

2. Hou, G.W., Taylor, A.C. III, and Korivi, V.M., "Discrete Shape Sensitivity Equations For Aerodynamic Problems," AIAA Paper 91-2259.

3. Taylor, A.C. III, Korivi, V.M., and Hou, G.W., "Sensitivity Analysis Applied to The Euler Equations: A Feasibility Study with Emphasis on Variation of Geometric Shape," AIAA Paper 91-0173, also, "A Taylor's Series Expansion of Geometric Shape Variation for The Euler Equations," to appear AIAA Journal, September 1992.

4. Taylor, A.C. III, Hou, G.W., and Korivi, V.M., "A Methodology for Determining Aerodynamic Sensitivity Derivatives With Respect to Variation of Geometric Shape," Proceedings of the AIAA/ASME/ASCE/AHS/ASC 32nd Structures, Structural Dynamics, and Materials Conference, April 8-10, Baltimore, MD, AIAA Paper 91-1101, also "A Methodology for Calculating Aerodynamic Sensitivity Derivatives," to appear, AIAA Journal.

5. Taylor, A.C., III, Korivi, V.M., and Hou, G.W. "Approximate Analysis and Sensitivity Analysis Methods For Viscous Flow Involving Variation of Geometric Shape," Proceedings of the AIAA 10th Computational Fluid Dynamics Conference, June 24-26, 1991, Honolulu, Hawaii, AIAA Paper 91-1569.

6. Taylor, A.C. III, Hou, G.W., and Korivi, V.M., "An Efficient Method For Estimating Steady-State Numerical Solutions to the Euler Equations", AIAA Paper 91-1680.

7. Korivi, V.M., "Sensitivity Analysis Applied to the Euler Equations," M.S. Thesis, Old Dominion University, Norfolk, VA, December, 1991.

8. Sorensen, T.M., "Viscous Airfoil Optimization Using Conformal Mapping Coefficients as Design Variables," M.S. Thesis, Department of Aeronautics and Astronautics, Massachusetts Institute of Technology, June, 1991.

9. Yates, E.C., Jr., and Desmarais, R., "Boundary Integral Method for Calculating Aerodynamic Sensitivities with Illustration for Lifting Surface Theory," in Proceedings of the International Symposium of Boundary Element Methods (IBEM 89), published by Springer-Verlag, Oct. 2-4, 1989, East Hartford, Conn.

10. Elbanna, H.M., and Carlson, L.A., "Determination of Aerodynamic Sensitivity Coefficients in the Transonic and Supersonic Regimes," Journal of Aircraft, Vol. 27, No. 6, June 1990, pp. 507-518, also AIAA Paper 89-0532.

11. Yates, E.C., Jr., "Aerodynamic Sensitivities From Subsonic, Sonic, and Supersonic Unsteady, Nonplanar Lifting-Surface Theory," NASA TM-100502, September, 1987.

12. Sobieszczanski-Sobieski, J., "The Case For Aerodynamic Sensitivity Analysis". In Sensitivity Analysis in Engineering, NASA CP-2457, 1987.

13. Bristow, D.R., and Hawk, J.D., "Subsonic Panel Method For The Efficient Analysis of Multiple Geometry Perturbations," NASA CP-3528, 1982.

14. Jameson, A., "Aerodynamic Design Via Control Theory," NASA CR-181749, also ICASE Report No. 88-64, November, 1988, also Journal of Scientific Computing, Vol. 3, pp. 233-260, 1988.

15. Frank P.D., and Shubin, G.R., "A Comparison of Optimization-Based Approaches for a Model Computational Aerodynamics Design Problem," Applied Mathematics Technical Report, ECA-TR-136-R1, Boeing Computer Services, Seattle, Washington, October, 1990, also to appear, Journal of Computational Physics.

16. Shubin, G.R., and Frank, P.D. "A Comparison of the Implicit Gradient Approach and the Variational Approach to Aerodynamic Design Optimization," Applied Mathematics and Statistics Technical Report, AMS-TR-163, Boeing Computer Services, Seattle, Washington, April, 1991.

17. Shubin, G.R., "Obtaining 'Cheap' Optimization Gradients from Computational Aerodynamics Codes", Applied Mathematics and Statistics Technical Report, AMS-TR-164, Boeing Computer Services, Seattle, Washington, June 1991.

18. Baysal, O. and Eleshaky, M.E., "Aerodynamic Sensitivity Analysis Methods for the Compressible Euler Equations," Recent Advances in Computational Fluid Dynamics, (ed. O. Baysal), ASME-FED Vol. 103, 11th Winter Annual Meeting, November, 1990, pp. 191–202.

19. Baysal, O., and Eleshaky, M.E., "Aerodynamic Design Optimization Using Sensitivity Analysis and Computational Fluid Dynamics," AIAA Paper 91-0471.

20. Baysal, O., Eleshaky, M.E., and Burgreen, G.W., "Aerodynamic Shape Optimization Using Sensitivity Analysis on Third-Order Euler Equations," Proceedings of the AIAA 10th Computational Fluid Dynamics Conference, June 24-26, 1991, Honolulu, Hawaii, AIAA Paper 91-1577.

21. Baldwin, B., and Lomax, H., "Thin-Layer Approximation and Algebraic Model for Separated Turbulent Flows," AIAA Paper 78–0257.

22. Walters, R.W., and Thomas, J.L., "Advances in Upwind Relaxation Methods," in State of the Art Surveys of Computational Mechanics, ed. A.K. Noor, pp. 145-183, ASME Publication, 1989, New York.

23. Thomas, J.L., Van Leer, B., and Walters, R.W., "Implicit Flux-Split Schemes for the Euler Equations," AIAA Journal, Vol. 28, No. 6, June 1990, pp. 973-974, also AIAA Paper 85-1680.

24. Walters, R.W., and Dwoyer, D.L., "An Efficient Iteration Strategy for Solution of the Euler Equations," AIAA Paper 85-1529.

25. Newsome, R.W., Walters, R.W., and Thomas, J.L., "An Efficient Iteration Strategy for Upwind/Relaxation solutions to the Thin-Layer Navier-Stokes Equations," AIAA Journal, Vol. 27, No. 9, September, 1989, pp. 1165-1166, also AIAA Paper 87–1113.

26. Thomas, J.L., and Walters, R.W., "Upwind Relaxation Algorithms for the Navier-Stokes Equations," AIAA Journal, Vol. 25, No. 4, April 1987, pp. 527–534.

27. Napolitano, M., and Walters, R.W., "An Incremental Block-Line-Gauss-Seidel Method for the Navier-Stokes Equations, AIAA Journal, Vol. 24, No. 5, May 1986, pp. 770–776.

28. Walters, R.W., and Dwoyer, D.I., "Efficient Solutions to the Euler Equations for Supersonic Flow with Embedded Subsonic Regions," NASA Technical Paper 2523, January 1987.

29. Van Leer, B., "Flux-Vector Splitting for the Euler Equations," ICASE Report 82–30, September 1982 (also Lecture Notes in Physics, Vol. 170, 1982, pp. 507–512).

30. Taylor, A.C. III, "Convergence Acceleration of Upwind Relaxation Methods For The Navier-Stokes Equations," Ph.D. Dissertation, Virginia Polytechnic Institute and State University, Blacksburg, VA, July, 1989.

31. Riggins, D.W., Walters, R.W., and Pelletier, D., "The Use of Direct Solvers for Compressible Flow Computations," AIAA Paper 88–0229.

32. Hafez, M., Palaniswamy, S., and Mariani, P., "Calculations of Transonic Flows with Shocks Using Newton's Method and Direct Solver, Part II," AIAA Paper 88–0226.

33. Venkatakrishnan, V., "Newton Solution of Inviscid and Viscous Problems", AIAA Journal Vol. 27, No. 7, July 1989, pp. 885–891, also AIAA Paper 88–0413.

34. Beam, R.M. and Warming, R.F., "An Implicit Factored Scheme for the Compressible Navier-Stokes Equations," AIAA Journal, Vol. 16, April 1978, pp. 393–402.

35. Taylor, A.C., III, Ng, W.F., and Walters, R.W., "Upwind Relaxation Algorithms for the Navier-Stokes Equations Using Inner Iterations," Proceedings of the AIAA 9th Computational Fluid Dynamics Conference, June 13-15, 1989, Buffalo, New York, AIAA Paper 89–1954, also Journal of Computational Physics, Vol. 99, No. 1, March 1992, pp. 68-78.

36. Walters, R.W., Dwoyer, D.L., and Hassan, H.A., "A Strongly Implicit Procedure for the Compressible Navier Stokes Equations," AIAA Journal, Vol. 24, No. 1, January 1986, pp. 6-12.

37. Ajmani, K., Ng, W.F., and Liou, M.S., "Generalized Conjugate-Gradient Methods for the Navier-Stokes Equations", Proceedings of the AIAA 10th Computational Fluid Dynamics Conference, June 24–26, 1991 Honululu, Hawaii, AIAA Paper 91–1556.

38. Venkatakrishnan, V., "Preconditioned Conjugate Gradient Method For The Compressible Navier-Stokes Equations", AIAA Journal, Vol. 29, No. 7, July, 1991, pp. 1092-1100, also AIAA Paper 90–0586.

39. Venkatakrishnan, V., NASA Ames Research Center, Private Communication.

40. Thomas, J.L, and Salas M.D., "Far-Field Boundary Conditions for Transonic Lifting Solutions to the Euler Equations", AIAA Journal Vol. 27, No. 7, July 1986, pp. 1074-1080, also AIAA Paper 85-0020.

41. Smith, R.E., Jr., and Sadrehaghighi, I., "Grid Sensitivity in Airplane Design," in Proceedings of the 4th International Symposium of Computational Fluid Dynamics, September 9–12 1991, University of California-Davis, pp. 1071–1077.

42. Smith, R.E., Jr., and Wiese, M.R., "Interactive Algebraic Grid-Generation Technique," NASA TP-2533, March 1986.

43. Rajan, S.D., and Belegundu, A.D. "A Shape Optimization Approach Using Fictitious Loads As Design Variables," Proceedings of the AIAA/ASME/ASCE/AHS 28th Structures, Structural Dynamics, and Materials Conferences," April 6-8, 1987, Monterey, CA, also AIAA Paper 87-0834.

44. Choi, K.K., and Yao, T.M., "3-D Modelling and Automatic Regridding in Shape Design Sensitivity Analysis," in Sensitivity Analysis in Engineering, NASA Conference Publication 2457, September, 1986, pp. 329-346.

45. Viviand, H., "Comparison of Numerical Solutions to Internal Flow in a Double-Throat Nozzle," GAMM Committee for Numerical Methods in Fluid Mechanics, France, December, 1985.

46. Thomas, J.L., Walters, R.W., Van Leer, B., and Rumsey, C.L., "An Implicit Flux-Split Algorithm for the Navier-Stokes Equations," GAMM Committee for Numerical Methods in Fluid Mechanics, France, December, 1985.

47. Bristeau, M.O., Glowinski, R., Periaux, J., and Viviand, Henri (Eds.), "Numerical Simulation of Compressible Navier-Stokes Flows," Notes on Numerical Fluid Mechanics, (Proceedings of a GAMM Workshop, Numerical Methods in Fluid Mechanics), Vol. 18, pp. 5–10, published by Friedr. Vieweg, & Sohn, Braunschweig, Germany, 1987.

48. Vanderplaats, G.N., "ADS- A Fortran Program for Automated Design Synthesis," NASA CR-177785, NASA Ames Research Center, September, 1985.

49. Korivi, V.M., Taylor, A.C. III, Newman, P.A., and Jones, H.E., "An Incremental Strategy For Calculating Consistent Discrete CFD Sensitivity Derivatives," NASA TM-104207, February, 1992. (also to be presented at the Fourth AIAA/USAF/NASA/OAI Symposium on Multidisciplinary Analysis and Optimization, September 21–23, 1992, Cleveland OH).

50. Newman, P.A., Hou, G.J.-W., Jones, H.E., Taylor, A.C. III, and Korivi, V.M., "Observations On Computational Methodologies For Use In Large-Scale Gradient-Based Multidisciplinary Design Incorporating Advanced CFD Codes," NASA TM-104206, February, 1992 (also to be presented at the Fourth AIAA/USAF/NASA/OAI Symposium on Multidisciplinary Analysis and Optimization, September 21-23, 1992, Cleveland, OH).

List of Illustrations

Fig. (1) – Nine-Point "Difference Stencil"
Representation Of Eq. (14) For A Typical Interior Cell.

$$\left(\left[\frac{1}{J\Delta t}\right] - \left[\frac{\partial R^n(Q)}{\partial Q}\right]\right)$$

$$^{n}\Delta Q = R^n(Q)$$

Fig. (2) – Illustration Of The Nine-Diagonal Banded
Structure Of The Global Coefficient Matrix Of Eq. (12)

Unit Load

▲ Symbol Indicates Simple Support, Zero Displacement.
(Points Supported Included Leading And Trailing Edges,
Points In Wake, And All Points At The Far-Field Boundary)

Fig. (3) – Illustration Of The "Elastic Membrane" Representation Of The Computational
Domain, Using The Fictitious Load Method For Computing Grid Sensitivity Derivatives.
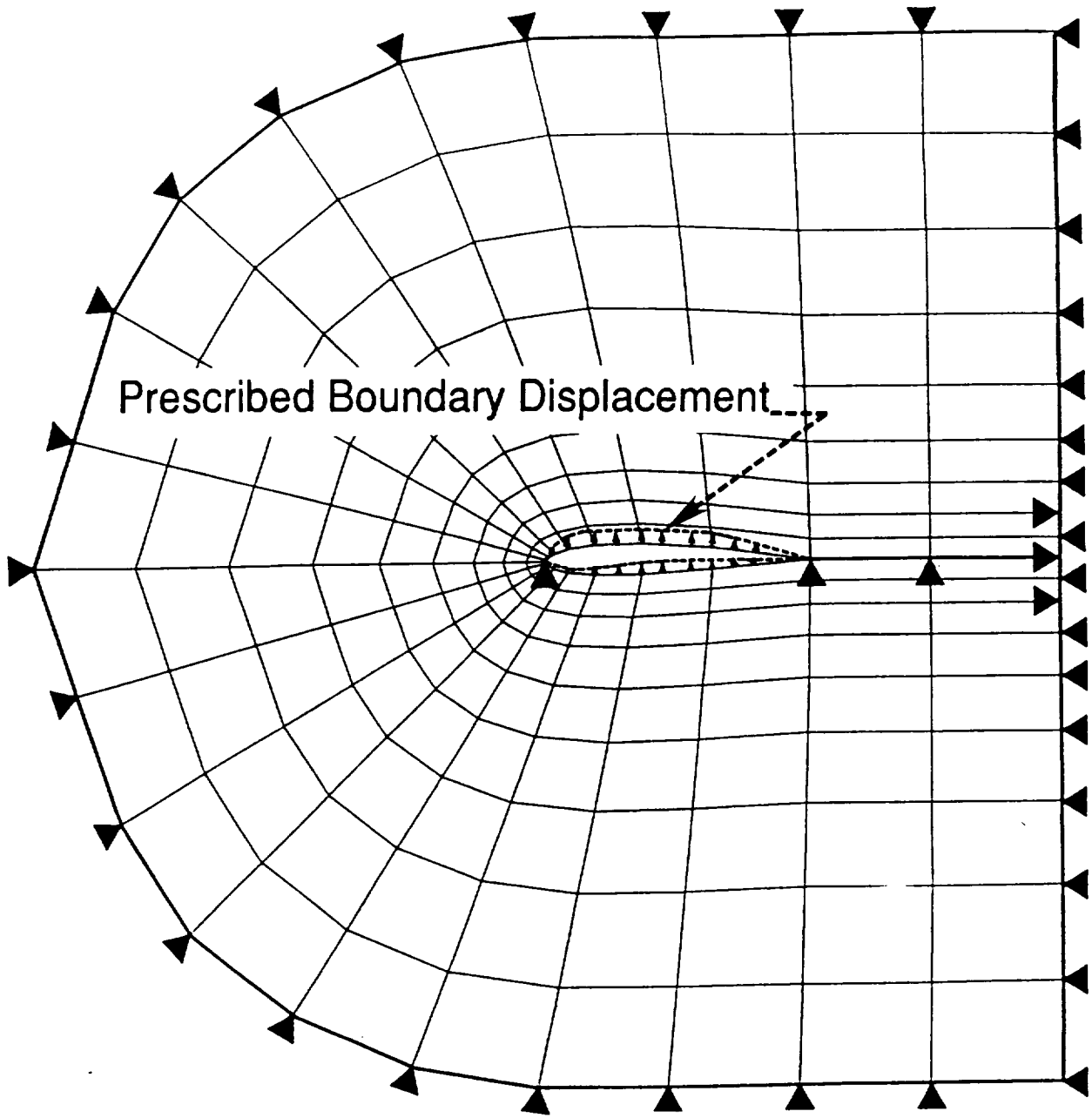
Prescribed Boundary Displacement

▲ Symbol Indicates Simple Support, Zero Displacement.
(Points Supported Included Leading And Trailing Edges,
Points In Wake, And All Points At The Far-Field Boundary)

Fig. (4) – Illustration Of The "Elastic Membrane" Representation
Of The Computational Domain Using The Prescribed Boundary
Displacement Method For Computing Grid Sensitivity Derivatives.

Fig. (5b) – Computational Mesh, 21×10 Points, Regridded Domain Using The "Elastic Membrane" Analogy, The Prescribed Displacement Method, And Eqs. (43) Through (45), For C=0.04, T=T$_o$=0.12, L=L$_o$=0

Fig. (5a) – Computational Mesh, 21×10 Points, "C" Mesh For A NACA 1412 Airfoil Using The Mesh Generation Code Of Ref. [42].
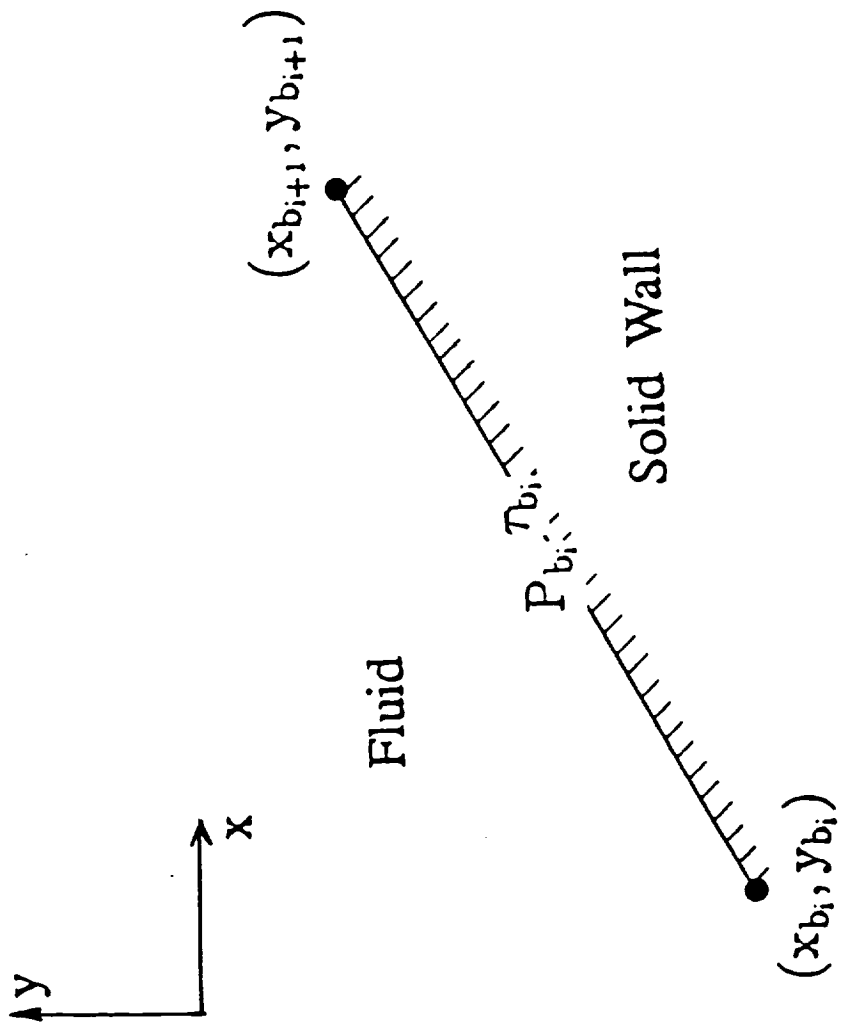
Fig. (6) — Illustration Of The ith Element On A Boundary.
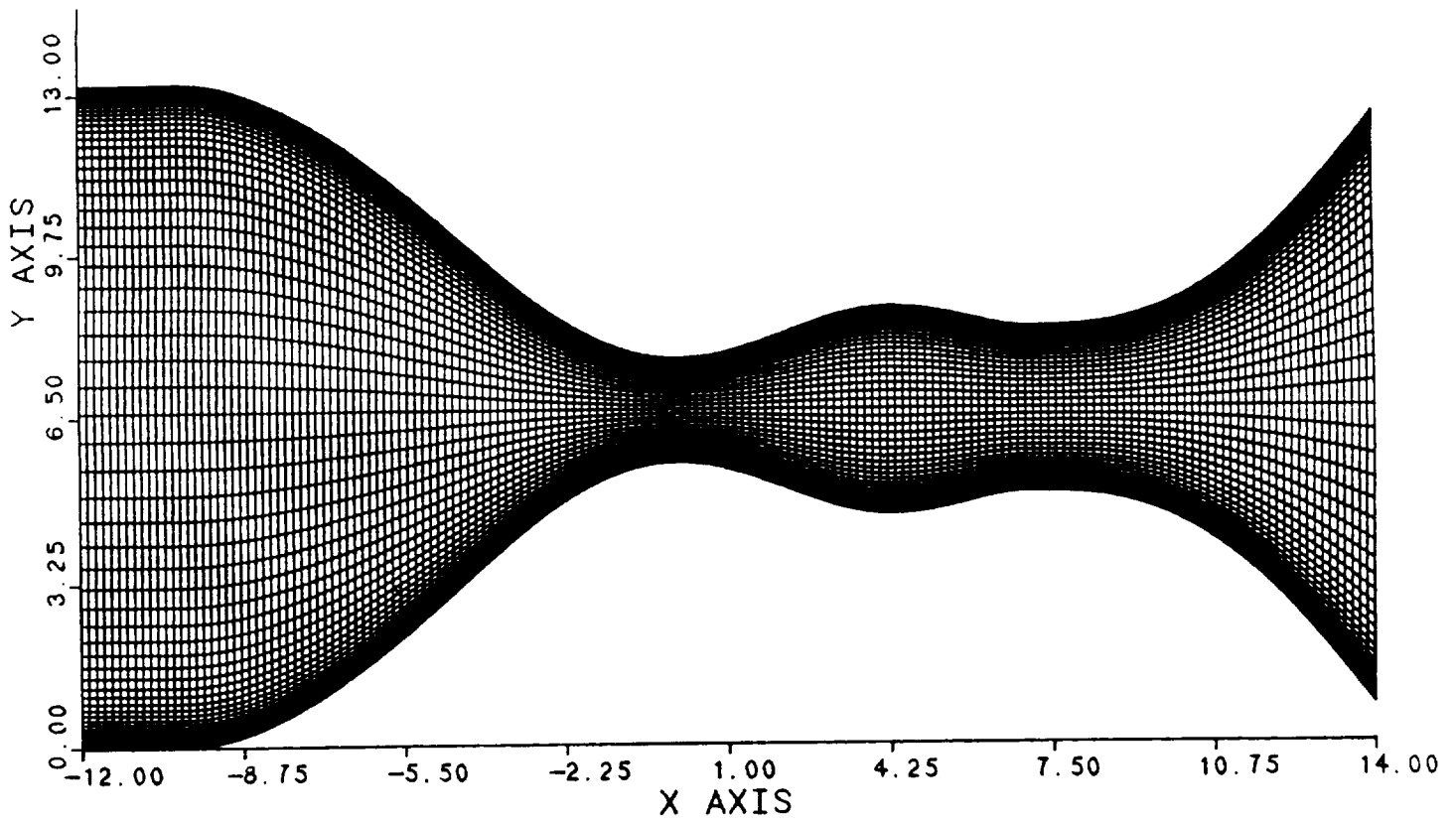
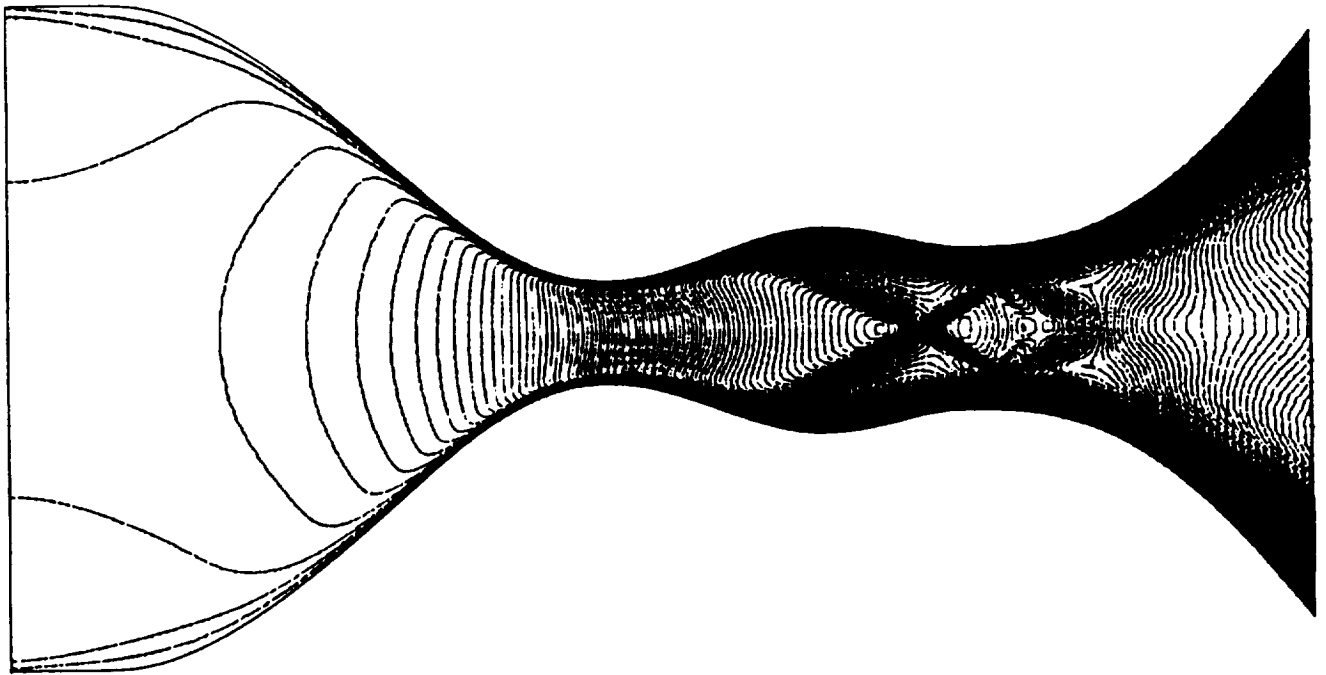Fig. (7) – Computational Mesh, 171×38 Points, Initial
Geometry of The Double-Throat Nozzle Problem.

Fig. (8) – Mach Contours For The Double-Throat Nozzle Problem, Initial Design.
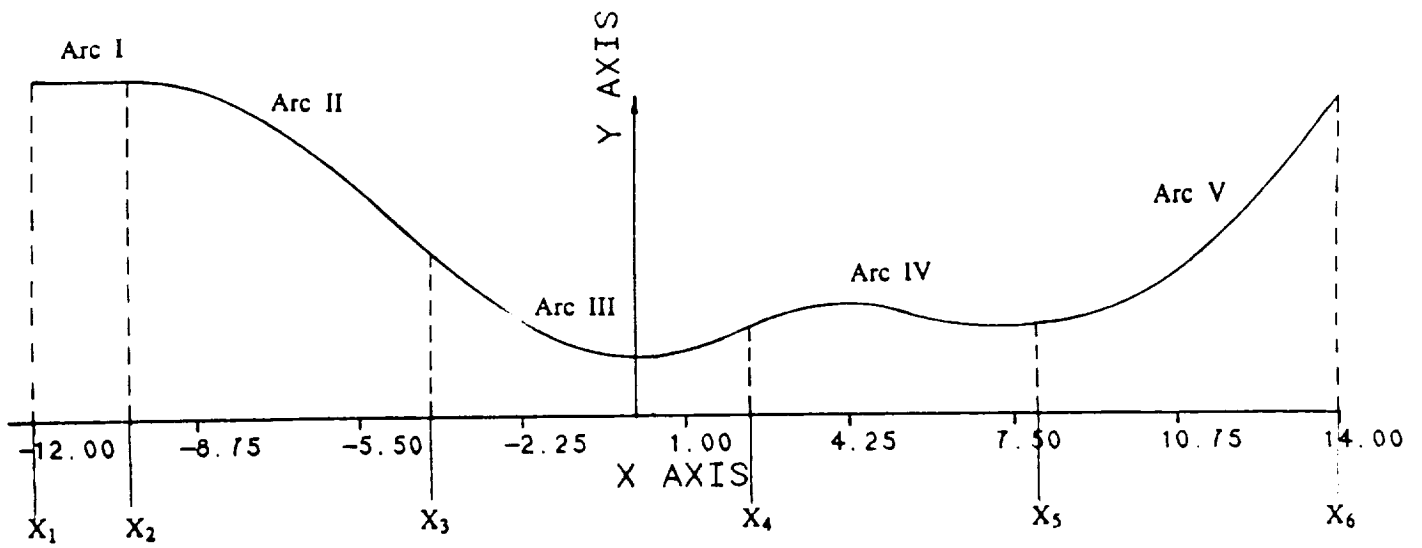
Fig. (9) Illustration Of The Parameterization Of The
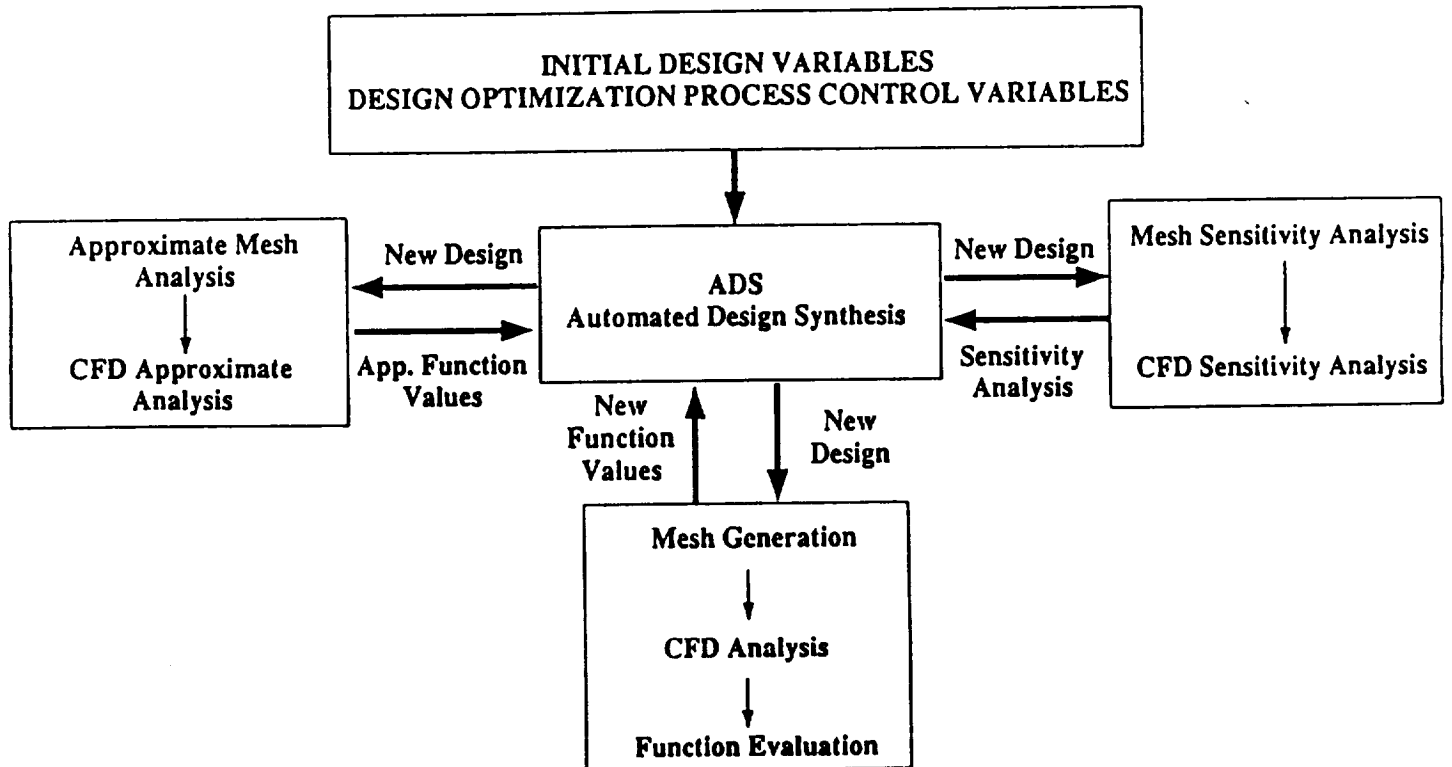Boundary Shape, Double-Throat Nozzle Problem.

Fig. (10) – Illustration of The Flow Chart For The Proposed
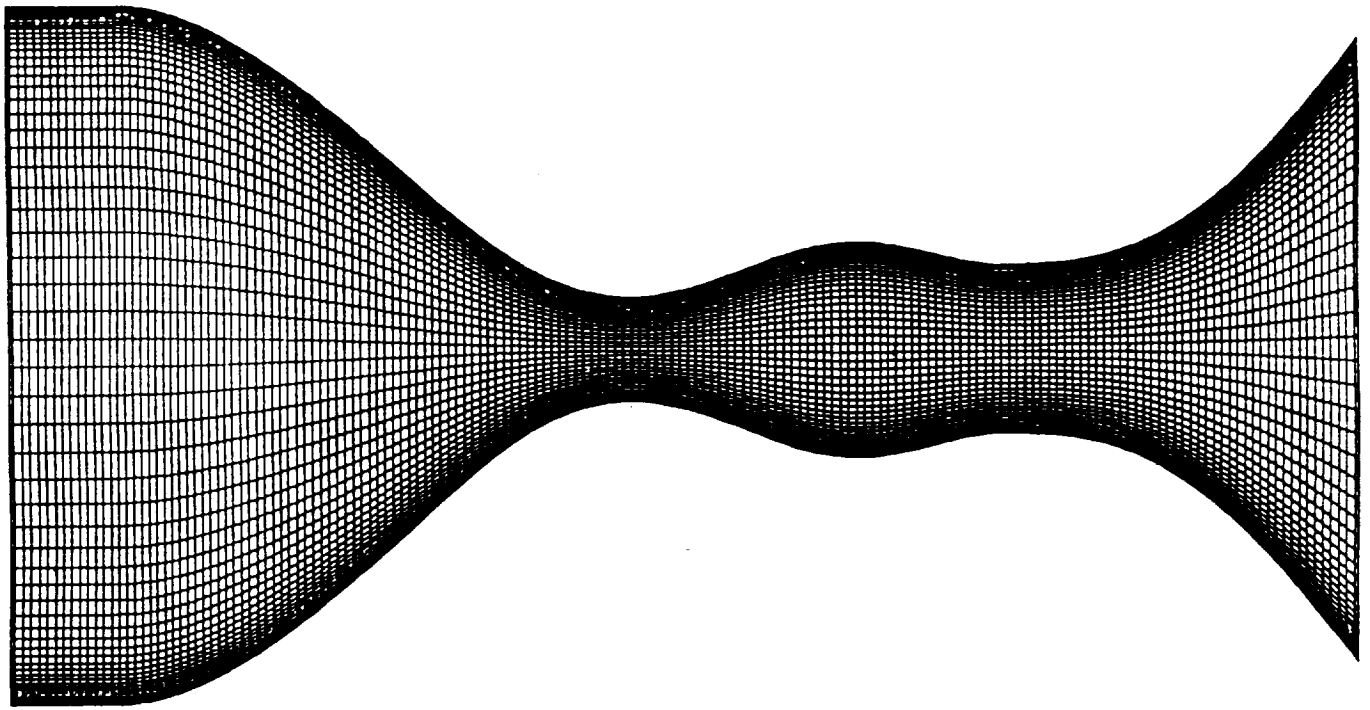Sensitivity Based Aerodynamic Shape Optimization Strategy.

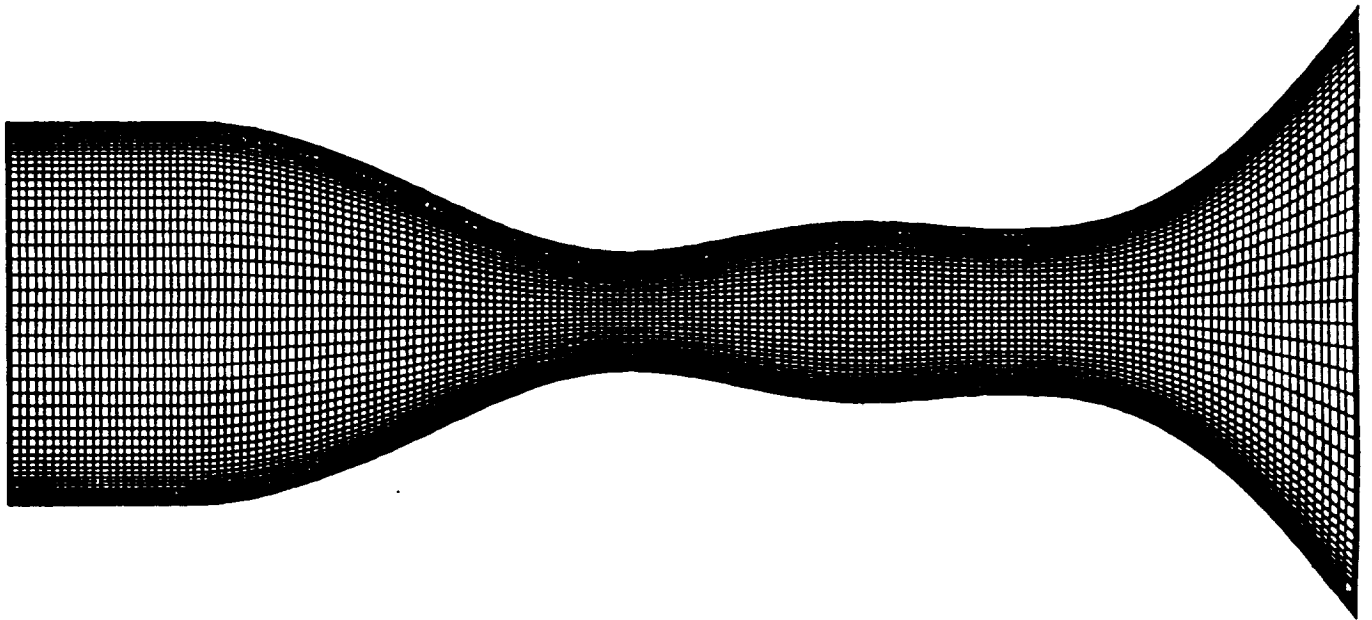Fig. (11a) – Illustration Of The Initial Design Of The Double-Throat Nozzle, C_x= +754.4

Fig. (11b) – Illustration Of The Final Design Of The Double-Throat Nozzle, C_x= +313.9

Fig. (12a) – Illustration Of The Initial Airfoil Design,
NACA 2412, M_∞ = 0.70, RE_L=5000, α=0.0°

Fig. (12b) – Illustration Of The Final Airfoil Design
Following Optimization, M_∞ =0.70, RE_L=5000, α=0.0°